CHAPTER III

RESULTS AND DISCUSSION

3.1 Concept of Molecular Design

It is well known that porphyrins and their metal complexes can be utilized as materials in various applications such as optoelectronic devices, dyes and pigments, photodynamic therapeutic agents, and molecular sensors. However, most of porphyrin derivatives display similar optical properties because their π-conjugation are limited in their core ring only. Therefore, the most interesting way to tune their optical properties is the extension of π-conjugated systems of porphyrins by connecting the porphyrin ring with π-conjugated linkers.

Owing to this reason, this research is aimed to synthesize an extensive series of novel alkyne-linked porphyrin metal complexes which exhibit higher π-conjugated length compared to non-conjugate-linked porphyrins. The general structure of target molecules is presented in **Figure 3.1**.

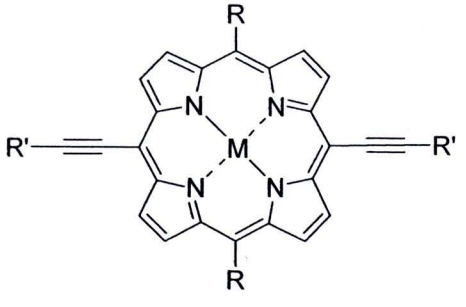

Figure 3.1 The general structure of target molecules

As shown in **Figure 3.1**, there are many parts in the structure including:

- R groups : these groups are connected at the *meso*-positions of porphyrin rings to improve the solubility of the chromophores which is an important factor in organic synthesis and fabrication process of materials. In this research, an *n*-hexyl group (as alkyl groups) and a mesityl group (as aryl groups) were chosen to be used in order to compare the solubility of their porphyrin derivatives.

- alkyne linkers : alkyne moieties are linked directly at the remaining *meso*-positions of porphyrin rings in order to extend the π-conjugated systems.

- R' groups : these groups consist of both electron withdrawing and electron donating groups. These are attached at the other side of the alkyne linkers so that the effect of substituents on photophysical properties of porphyrins can be studied.

- M : M are metal ions such as zinc(II) or manganese(II) which will be introduced to the ring to make corresponding porphyrin metal complexes. These are two hydrogen atoms in the case of free base porphyrins. With this modification the effect of metal ions on photophysical and coordination properties of porphyrins can be determined.

3.2 Synthesis of Porphyrin Building Blocks

The prior step for the synthesis of alkyne-linked porphyrin metal complexes is the preparation of *meso*-dibrominated porphyrins as porphyrin building blocks. These derivatives of dihexylporphyrin and dimesitylporphyrin were prepared based on the general synthetic strategy as illustrated in **Figure 3.2**.

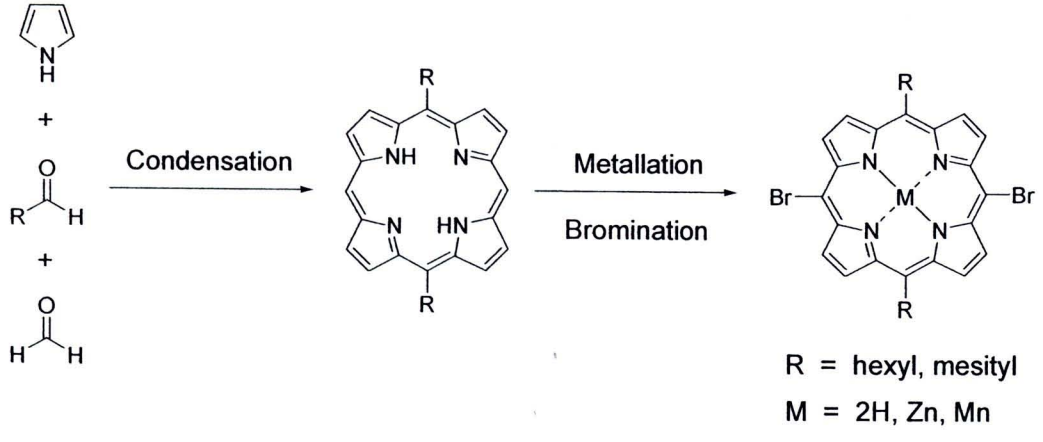

Figure 3.2 The general synthetic strategy for the preparation of *meso*-dibrominated porphyrins as porphyrin building blocks

The first step of this strategy involves the formation of 5,15-disubstituted porphyrins from the reaction of pyrrole with formaldehyde and another aldehyde (heptaldehyde or mesitaldehyde). After that, the corresponding 5,15-disubstituted porphyrins will be used as starting materials for the preparation of *meso*-dibrominated porphyrin metal complexes by metallation and brominaion reaction.

3.2.1 Synthesis of *meso*-Dihexylporphyrin Derivatives

3.2.1.1 Synthesis of 5,15-Dihexylporphyrin (DHP, 13)

As shown in **Figure 3.3**, there are three pathways to synthesize 5,15-dihexylporphyrin from pyrrole and two aldehydes: formaldehyde and heptaldehyde.

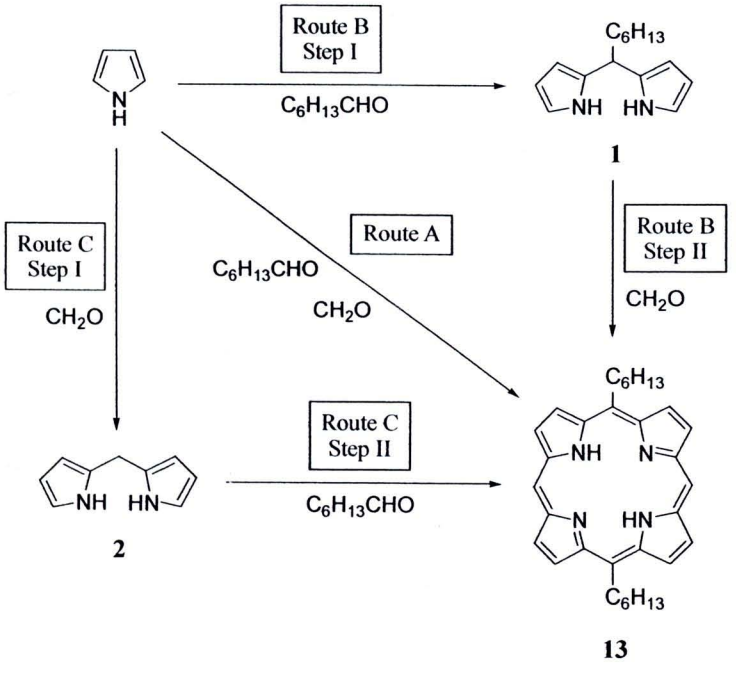

Figure 3.3 The synthetic pathways of 5,15-dihexylporphyrin

Route A : *Synthesis of 5,15-Dihexylporphyrin via Monopyrrole Tetramerization*

This synthetic route presented itself as the easiest pathway for the preparation of 5,15-dihexylporphyrin because of its one-pot nature. All of starting materials including pyrrole, formaldehyde, and heptaldehyde were reacted in one step in the presence of $BF_3.OEt_2$ as catalyst followed by oxidation with DDQ. After a workup by short silica column, a mixture of hexylporphyrin derivatives was obtained and isolated by flash column chromatography using hexanes as mobile phase. Each of the fractions from column chromatography was monitored preliminarily by TLC. The TLC results indicated that the mixture of hexylporphyrins could not be completely separated because each component in the mixture has similarly close chromatographic R_f values.

Furthermore, MALDI-TOF mass spectrometry was used to characterize each fraction from column chromatography compared to the exact mass of predicted porphyrin components in the mixture (**Figure 3.4**).

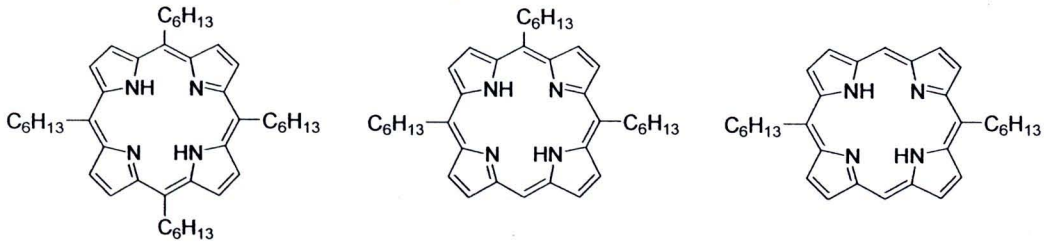

5,10,15,20-THP
m/z : 646.497

5,10,15-THP
m/z : 562.404

5,15-DHP
m/z : 478.310

5,10-DHP
m/z : 478.310

5-HP
m/z : 394.216

Porphine
m/z : 310.122

Figure 3.4 Structures and exact masses of predicted porphyrin components in the hexylporphyrin mixture

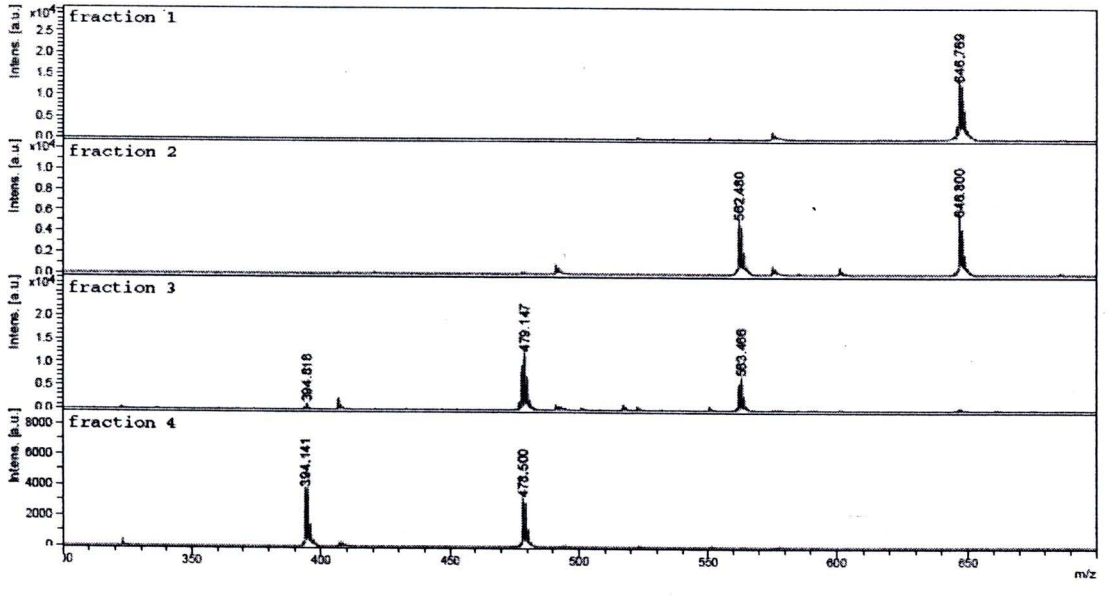

Figure 3.5 The MALDI-TOF mass spectroscopic data of each fraction from column chromatography of the hexylporphyrin mixture

The MALDI-TOF mass spectroscopic data in **Figure 3.5** revealed that only 5,10,15,20-tetrahexylporphyrin could be isolated from the mixture (**Figure 3.5, Fraction 1**), while 5,15-dihexylporphyrin could not be isolated from other components (**Figure 3.5, Fraction 3**) and porphine could not be found in the spectra. From these results, it could be concluded that route A was not a suitable pathway to synthesize 5,15-dihexylporphyrin.

Route B : *Synthesis of 5,15-Dihexylporphyrin from 5-Hexyldipyrromethane*

This strategic route is divided in two steps. The first step (Step I) is the preparation of 5-hexyldipyrromethane and the second step (Step II) is the synthesis of 5,15-dihexylporphyrin by reaction of 5-hexyldipyrromethane and formaldehyde.

Step I : *Synthesis of 5-Hexyldipyrromethane*

5-Hexyldipyrromethane was prepared according to a literature method [53]. Typically, 5-hexyldipyrromethane was performed by the reaction of heptaldehyde with 25 equivalents of pyrrole in the presence of TFA at room temperature without solvent.

Step II : *Synthesis of 5,15-Dihexylporphyrin from 5-Hexyldipyrromethane*

Unfortunately, attempts to synthesize 5,15-dihexylporphyrin by the condensation of 5,15-dipyrromethane with 37% formaldehyde solution using TFA or $BF_3.OEt_2$ as acid catalyst followed by oxidation with DDQ failed to give the desired product.

Route C : *Synthesis of 5,15-Dihexylporphyrin from Dipyrromethane*

Similar to route B, this strategic route is divided in two steps. The first step (Step I) is the preparation of dipyrromethane and the second step (Step II) is the synthesis of 5,15-dihexylporphyrin by reaction of dipyrromethane and heptaldehyde.

Step I : *Synthesis of Dipyrromethane*

Generally, dipyrromethane was synthesized by a condensation of excess pyrrole and paraformaldehyde in the presence of an acid catalyst without solvent. However, paraformaldehyde is relatively insoluble in neat pyrrole at room temperature. Consequently, it was necessary to heat the reaction mixture to 55 °C in

order to increase the solubility of paraformaldehyde sufficiently to enable rapid condensation and give a good yield of dipyrromethane [53].

To optimize the condition for dipyrromethane synthesis, effects of acid catalysts and pyrrole:paraformaldehyde ratio were examined.

Effects of two different acids (TFA and $MgBr_2$) on the condensation with a 25:1 ratio of pyrrole and paraformaldehyde are listed in **Table 3.1**. These observations presented that TFA as Bronsted acid could readily catalyze the reaction within a short time, but gave a low yield of dipyrromethane and resulted in darkening of the product. On the other hand, $MgBr_2$ as Lewis acid gave a better yield and less darkening of the product. These results were consistent with the preparation of 5-phenyldipyrromethane which was reported in the previous literature [57]. Due to better results of $MgBr_2$ in terms of yield and appearance of the product, $MgBr_2$ was selected as the catalyst for the formation of dipyrromethane.

Table 3.1 Effects of acids on the condensation with a 25:1 ratio of pyrrole and paraformaldehyde

	TFA	$MgBr_2$
Type of acid	Bronsted acid	Lewis acid
Solubility in reaction mixture	soluble	insoluble
Reaction time	10 min	3 h
%Yield	19	36
Appearance of product	black solid	brown solid

Next, the effect of pyrrole:paraformaldehyde ratio on the yield of dipyrromethane was also examined and summarized in **Table 3.2**. The reaction in this study was performed using $MgBr_2$ as catalyst under N_2 at 55 ^{o}C and the ratio of pyrrole:paraformaldehyde was varied ranging from 10:1 to 25:1. These results indicated that upon increasing the pyrrole:paraformaldehyde ratio in combination with decreasing the reaction time, higher yield of dipyrromethane was obtained. A possible reason for these results was that the high concentration of pyrrole and short reaction time decreased the formation of higher oligomers of pyrrole and afforded dipyrromethane as the major product.

Table 3.2 Effect of pyrrole:paraformaldehyde ratio and reaction time on the yield of dipyrromethane

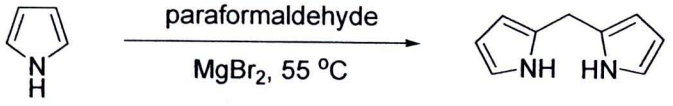

2

Entry	Pyrrole:paraformaldehyde	Time	Yield (%)
1	25:1	3 h	36
2	20:1	4 h	32
3	15:1	5 h	28
4	10:1	6 h	22

From the survey of optimum condition for the preparation of dipyrromethane, the condensation with a 25:1 ratio of pyrrole and paraformaldehyde using $MgBr_2$ as catalyst under N_2 at 55 °C for 3 h was chosen. Under this condition, the crude mixture composed of unreacted pyrrole, dipyrromethane, and tripyrrane was obtained and characterized by ^1H NMR spectroscopy (**Figure 3.6**). Unreacted pyrrole was removed and recovered by evaporation under vacuum. Later, dipyrromethane and tripyrrane were separated by column chromatography using hexanes:CH_2Cl_2:EtOAc (7:2:1) as mobile phase. Desired dipyrromethane was collected as brown solid and small colorless clear crystals which could not be remedied the darkening of product by recrystallization or silica pad filtration.

Step II : *Synthesis of 5,15-Dihexylporphyrin from Dipyrromethane*

5,15-Dihexylporphyrin was synthesized by reaction of dipyrromethane with heptaldehyde in the presence of $BF_3.OEt_2$ in $CHCl_3$ and then DDQ was added to oxidize porphyrinogen intermediate to porphyrin product. The residual DDQ and tar were removed by short silica column to obtain 5,15-dihexylporphyrin as dark purple solid in moderate yield (23%). The product was then characterized by ^1H NMR spectroscopy and MALDI-TOF mass spectrometry.

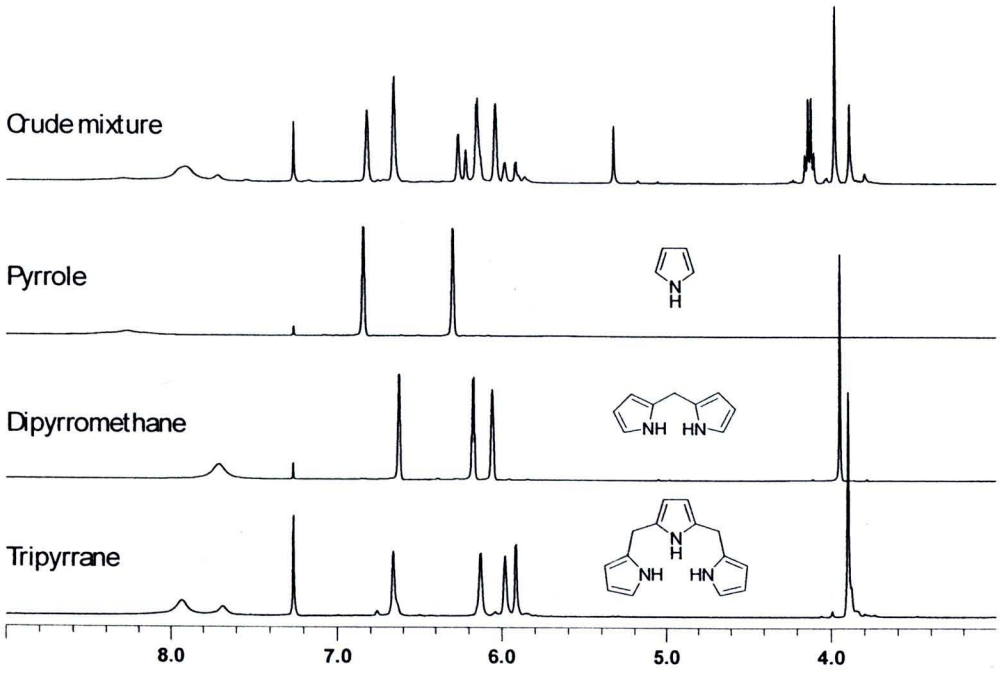

Figure 3.6 The ^{1}H NMR spectra of crude mixture, pyrrole, dipyrromethane, and tripyrrane

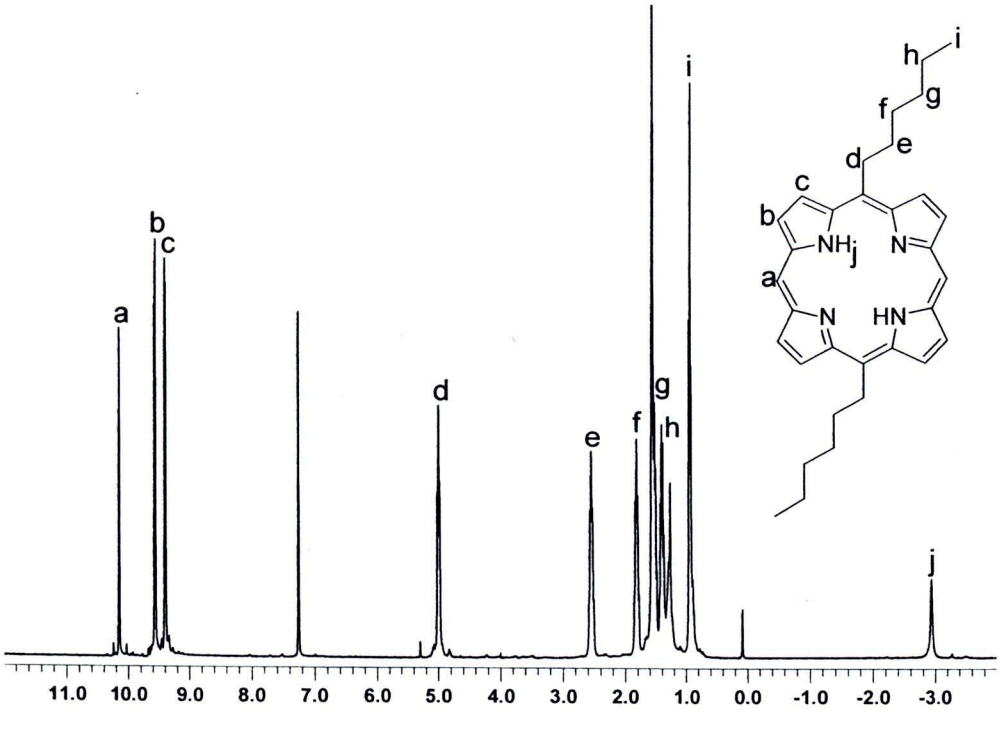

Figure 3.7 The ^{1}H NMR spectrum of 5,15-dihexylporphyrin (DHP, **13**)

The ^{1}H NMR spectrum of 5,15-dihexylporphyrin exhibited signals of protons corresponding to the structure as shown in **Figure 3.7**. There were 3 signals in the aromatic region. The first signal at δ 10.16 ppm corresponded to the 2 *meso*-porphyrin protons and the other two signals at δ 9.40 and 9.57 ppm corresponded to *β*-porphyrin protons. The signals of protons in the hexyl side chain groups were observed at chemical shifts ranging from δ 0.94 to 5.00 ppm. Moreover, an upfield singlet signal was found at δ -2.94 ppm which refered to internal N-H protons within the inner core of porphyrin ring. This signal is the characteristic peak of free base porphyrin. Not only ^{1}H NMR spectrum but MALDI-TOF mass spectrum was also used to characterize the product. Molecular ion peak was found at 479.400 which was consistent with calculated exact mass of 5,15-dihexylporphyrin at 478.310.

The results described in each pathway suggested that route C is the best pathway to synthesize 5,15-dihexylporphyrin. Although two steps were needed in this pathway, it provided the desired product in satisfactory yield without the formation of other porphyrins.

3.2.1.2 Synthesis of (5,15-Dihexylporphyrinato)zinc(II) (Zn-DHP, 14)

To prepare (5,15-dihexylporphyrinato)zinc(II) (Zn-DHP, **14**), a saturated solution of $Zn(OAc)_2.2H_2O$ in methanol was added to a refluxing solution of 5,15-dihexylporphyrin in $CHCl_3$. Zinc(II) ion was inserted easily into the core of free base 5,15-dihexylporphyrin as indicated by a change in the color of the solution from purple to bright red. After a workup, red solid of Zn-DHP was obtained in a quantitative yield (96%). The structure of product was determined by ^{1}H NMR spectroscopy and MALDI-TOF mass spectrometry.

The ^{1}H NMR spectrum of Zn-DHP showed relatively similar ^{1}H NMR signals to that of free base 5,15-dihexylporphyrin with slightly shifted peaks. However, the characteristic signal of the internal N-H protons in the spectrum of free base 5,15-dihexylporphyrin at δ -2.94 ppm had disappeared because of the insertion of zinc(II) ion. In addition, MALDI-TOF mass analysis was also used to confirm the structure of Zn-DHP with the molecular ion peak found at 540.359 which was consistent with calculated exact mass of 540.223.

3.2.1.3 Synthesis of 5,15-Dibromo-10,20-dihexylporphyrin (Br_2DHP, 15)

5,15-Dibromo-10,20-dihexylporphyrin (Br_2DHP, **15**) was synthesized readily from bromination reaction of 5,15-dihexylporphyrin with 2 equivalents of NBS. After recrystallization of product with CH_2Cl_2/MeOH system, Br_2DHP was afforded as a purple solid in 79% yield. This product showed lower solubility in CH_2Cl_2 and $CHCl_3$ compared to 5,15-dihexylporphyrin but it can be completely soluble in THF. Characterization by ^1H NMR spectroscopy and MALDI-TOF mass spectrometry were carried out.

Most of ^1H NMR signals of Br_2DHP were found at similar positions to that of 5,15-dihexylporphyrin. Nevertheless, the successful bromination at two *meso*-positions of 5,15-dihexylporphyrin led to the complete absence of *meso*-protons signal at δ 10.16 ppm. The MALDI-TOF mass spectrum showed the molecular ion peak at 636.555 which was consistent with calculated exact mass of 634.131.

3.2.1.4 Synthesis of (5,15-Dibromo-10,20-dihexylporphyrinato)zinc(II) (Zn-Br_2DHP, 16)

Similar to the preparation of Zn-DHP, (5,15-Dibromo-10,20-dihexyl-porphyrinato)zinc(II) (Zn-Br_2DHP, **16**) was prepared by refluxing Br_2DHP with a saturated solution of $Zn(OAc)_2.2H_2O$ in methanol. After the reaction was complete, the color of solution was changed from red-brown to blue-green. When the refluxed solution was cooled down and let stand for 1 hour, the brown precipitate surprisingly occurred and the blue-green color of the solution has faded to colorless. The main reason of this result may be because of the poor solubility of product in $CHCl_3$. Then, the precipitate of product was collected on a filter, washed with cold methanol, and characterized by ^1H NMR spectroscopy and MALDI-TOF mass spectrometry.

On account of the poor solubility of product, characterization of Zn-Br_2DHP by ^1H NMR spectroscopy in $CDCl_3$ was not successful. Therefore, the solvent for NMR characterization of this product was changed to DMSO-d_6. As a result, the ^1H NMR spectrum was performed and showed signals of β-protons at δ 9.64 and 9.67 ppm and signals of protons on hexyl groups at δ 0.89-4.96 ppm. In order to confirm the formation of Zn-Br_2DHP, MALDI-TOF mass spectrometric data was used. The

molecular ion peak of Zn-Br_2DHP was found at 698.623 corresponding to calculated exact mass of Zn-Br_2DHP at 696.044.

Table 3.3 The ^{1}H NMR chemical shifts of *meso*-dihexylporphyrin derivatives

Porphyrins	Solvents	Chemical shifts			
		meso-protons	*β*-protons	hexyl protons	internal N-H protons
DHP, **13**	$CDCl_3$	10.16	9.40, 9.57	0.93, 1.40, 1.52, 1.82, 2.54, 5.00	-2.94
Zn-DHP, **14**	$CDCl_3$	10.09	9.40, 9.65	0.96, 1.42, 1.55, 1.88, 2.58, 5.03	-
Br_2DHP, **15**	$CDCl_3$	-	9.42, 9.68	0.93, 1.40, 1.50, 1.78, 2.47, 4.87	-2.67
Zn-Br_2DHP, **16**	DMSO-d_6	-	9.64, 9.67	0.89, 1.34, 1.46, 1.76, 2.40, 4.96	-

3.2.2 Synthesis of *meso*-Dimesitylporphyrin Derivatives

3.2.2.1 Synthesis of 5,15-Dimesitylporphyrin (DMP, 17)

Employing the same synthetic protocol of 5,15-dihexylporphyrin as described before, 5,15-dimesitylporphyrin was also synthesized from the reaction of dipyrromethane with mesitaldehyde using $BF_3.OEt_2$ as catalyst and DDQ as oxidizing agent. The product was obtained as a dark purple solid in satisfactory yield (40%) and subsequently characterized by ^{1}H NMR spectroscopy and MALDI-TOF mass spectrometry.

The ^{1}H NMR spectrum of 5,15-dimesitylporphyrin showed signals which was consistent with the structure depicted in **Figure 3.8**. The *meso*-proton signal was found at δ 10.23 ppm, while the *β*-proton signals were found at δ 8.89 and 9.93 ppm. Moreover, a series of proton signals of dimesityl groups was observed at δ 7.33 ppm of aromatic protons, 2.67 ppm of protons in two methyl groups at *para*-positions of phenyl rings, and 1.85 ppm of protons in four methyl groups at *ortho*-positions of phenyl rings. The extraordinarily upfield singlet signal at δ -3.06 ppm resulted from ring current effect was assigned to the internal N-H protons in the core of porphyrin rings. In addition, MALDI-TOF mass spectrum confirmed the structure by showing the molecular ion peak at 546.392. This was consistent with calculated exact mass of 5,15-dimesitylporphyrin at 546.278.

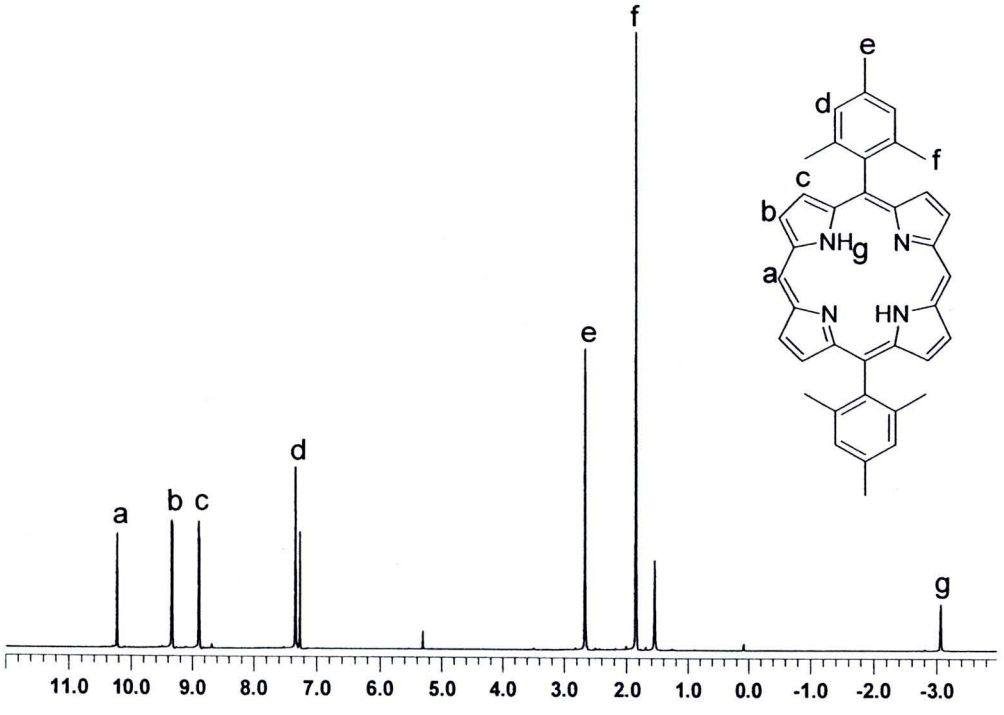

Figure 3.8 The ^{1}H NMR spectrum of 5,15-dimesitylporphyrin (DMP, **17**)

3.2.2.2 Synthesis of (5,15-Dimesitylporphyrinato)zinc(II) (Zn-DMP, 18)

The synthesis of (5,15-dimesitylporphyrinato)zinc(II) (Zn-DMP, **18**) using a saturated solution of $Zn(OAc)_2.2H_2O$ in methanol was carried out in a boiling $CHCl_3$ solution of 5,15-dimesitylporphyrin. Within 1 hour, the color of the solution was changed from purple to red as a result of the metallation of zinc(II) ion into the core of porphyrin ring. After a workup, red solid of Zn-DMP was yielded in 98%. The structure was confirmed by ^{1}H NMR spectroscopy and MALDI-TOF mass spectrometry.

The ^{1}H NMR spectrum of Zn-DMP showed most of proton signals similar to that of free base 5,15-dimesitylporphyrin. In contrast, the disappearance of the internal N-H proton signal at δ -3.06 ppm indicated the replacement of these protons with zinc(II) ion. The MALDI-TOF mass spectrum showed the molecular ion peak at 608.341 which was consistent with calculated exact mass of 608.192.

3.2.2.3 Synthesis of (5,15-Dimesitylporphyrinato)manganese(II) (Mn-DMP, 19)

The synthesis of (5,15-dimesitylporphyrinato)manganese(II) (Mn-DMP, **19**) using a saturated solution of $Mn(OAc)_2.4H_2O$ in methanol was carried out in a boiling DMF solution of 5,15-dimesitylporphyrin. The reaction was complete within 2 hour and the color of the solution was changed from purple to dark green. After a workup, a dark brown solid of Zn-DMP was obtained in 88% yield and characterized by ^1H NMR spectroscopy and MALDI-TOF mass spectrometry.

Unlike the ^1H NMR spectrum of Zn-DMP, that of Mn-DMP showed large broad peaks of proton resonances in both aromatic region and alkyl region which made it difficult to characterize. This is because manganese(II) ion is a paramagnetic metal ion which affect the NMR measurement. Nevertheless, the characteristic signal of internal N-H protons of free base 5,15-dimesitylporphyrin at δ -3.06 ppm was absent, supporting that manganese(II) ion had replaced these internal protons. Furthermore, the molecular ion peak at 599.532 was found in the MALDI-TOF mass spectrum corresponding to calculated exact mass of Mn-DMP at 599.201.

3.2.2.4 Synthesis of (5,15-Dibromo-10,20-dimesitylporphyrinato)-zinc(II) (Zn-Br_2DMP, 20)

To prepare (5,15-Dibromo-10,20-dimesitylporphyrinato)zinc(II) (Zn-Br_2DMP, **20**), Zn-DMP was treated with 2 equivalents of NBS in CH_2Cl_2 at 0 °C for 10 minutes. Then, the product was formed as purple precipitates after addition of MeOH and evaporation. The bromination under this condition proceeded with high regioselectivity, exclusively affording only *meso*-disubstituted porphyrin Zn-Br_2DMP in high yield (96%) without the formation of monosubstituted and *β*-substituted porphyrins. This could be confirmed by ^1H NMR spectroscopy and MALDI-TOF mass spectrometry.

The ^1H NMR spectrum of Zn-Br_2DMP exhibited only *β*-proton signals at δ 8.79 and 9.67 ppm whereas *meso*-proton signal had disappeared because of the complete bromination at the *meso*-positions of the porphyrin ring. Moreover, the proton signals of mesityl groups were found at δ 1.81, 2.65, and 7.29 ppm. The

MALDI-TOF mass spectrum showed the molecular ion peak at 766.601 which was consistent with calculated exact mass of 764.013.

3.2.2.5 Synthesis of (5,15-Dibromo-10,20-dimesitylporphyrinato)-manganese(II) (Mn-Br_2DMP, 21)

Attempts have been made to synthesize (5,15-Dibromo-10,20-dimesityl-porphyrinato)manganese(II) (Mn-Br_2DMP, **21**) by reacting Mn-DMP with 2 equivalents of NBS according to the synthesis of Zn-Br_2DMP. This resulted in an incomplete reaction detected by MALDI-TOF molecular ion peaks even though the reaction was carried out for a long time. Consequently, the condition of the reaction was modified by increasing the amount of NBS from 2 equivalents to 5 equivalents and extending the reaction time. As a result, the reaction was complete within 30 minutes to give the dibrominated porphyrin Mn-Br_2DMP as a dark green solid in high yield (95%). The product was characterized by ^{1}H NMR spectroscopy and MALDI-TOF mass spectrometry.

Similar to the ^{1}H NMR spectrum of Mn-DMP, that of Mn-Br_2DMP was not resolved due to the paramagnetic property of manganese(II) ion. In order to characterize the structure of Mn-Br_2DMP, MALDI-TOF mass spectrum was considered. It showed the molecular ion peak at 757.934 corresponding to calculated exact mass of Mn-Br_2DMP at 755.022.

Table 3.4 The ^{1}H NMR chemical shifts of *meso*-dimesitylporphyrin derivatives

Porphyrins	Solvents	Chemical shifts			
		meso-protons	β-protons	mesityl protons	internal N-H protons
DMP, **17**	$CDCl_3$	10.23	8.89, 9.33	1.85, 2.67, 7.33	-3.06
Zn-DMP, **18**	$CDCl_3$	10.25	8.97, 9.39	1.83, 2.67, 7.33	-
Mn-DMP, **19**[a]	$CDCl_3$	-	-	-	-
Zn-Br_2DMP, **20**	$CDCl_3$	-	8.79, 9.67	1.81, 2.65, 7.29	-
Mn-Br_2DMP, **21**[a]	$CDCl_3$	-	-	-	-

[a] The ^{1}H NMR spectra of porphyrin manganese(II) complexes were difficult to identify.

3.2.3 Solubility of Porphyrin Building Blocks

Solubility is an essential factor for carrying out synthetic transformations, purification procedures, diverse physical investigations, and fabrication processes. The solubility problem is significant with large planar aromatic compounds such as phthalocyanines, porphyrins, and their derivatives. Moreover, this problem exacerbates in arrays composed of multiple porphyrins in defined architectures [58]. Based on this information, the most prevalent *meso*-substituents of porphyrins have been employed to increase the solubility over that of *meso*-tetraphenylporphyrins such as pentyl [59], isopropyl [60], cyclohexyl [61], and 3,5-di-*tert*-butylphenyl [62] groups.

In order to find the appropriate substituent, heptaldehyde and mesitaldehyde which are inexpensively available aldehydes were chosen to use as starting materials for the synthesis of porphyrin building blocks. Then, the solubility of their porphyrin derivatives were compared as summarized in **Table 3.5**.

Table 3.5 The solubility of *meso*-dihexylporphyrin and *meso*-dimesitylporphyrin derivatives in common organic solvents

Porphyrins	Hexane	Et_2O	CH_2Cl_2	THF	$CHCl_3$	EtOAc
DHP, **13**	+ +	+ +	+ + +	+ + +	+ + +	+
Zn-DHP, **14**	-	+ +	+ + +	+ + +	+ + +	+
Br_2DHP, **15**	-	-	+	+ + +	+ +	-
Zn-Br_2DHP, **16**	-	-	-	+ + +	+ +	-
DMP, **17**	+	+ +	+ + +	+ + +	+ + +	+
Zn-DMP, **18**	+	+ +	+ + +	+ + +	+ + +	+ + +
Mn-DMP, **19**	+	+ +	+ + +	+ + +	+ + +	+ + +
Zn-Br_2DMP, **20**	+	+	+ + +	+ + +	+ + +	+ +
Mn-Br_2DMP, **21**	+	+ +	+ + +	+ + +	+ + +	+ + +

+ + + completely soluble; + + mostly soluble; + slightly soluble; - insoluble

The results from **Table 3.5** revealed that *meso*-dimesitylporphyrin derivatives showed better solubility in common organic solvents than *meso*-dihexylporphyrin derivatives. Interestingly, Zn-Br_2DHP exhibited the lowest solubility among of all observed porphyrins. On the other hand, Zn-Br_2DMP could be soluble in various organic solvents especially in CH_2Cl_2, $CHCl_3$, and THF.

The main reason of these results may be attributed to π-π stacking interactions between porphyrin molecules (**Figure 3.9**). In the case of Zn-Br_2DHP, each molecule can be stacked closely because hexyl groups have not enough steric hindrances. In contrast, mesityl groups in Zn-Br_2DMP are relatively bulky groups twisted out of the plane of porphyrins leading to decreasing π-π stacking interactions and increasing the solubilty.

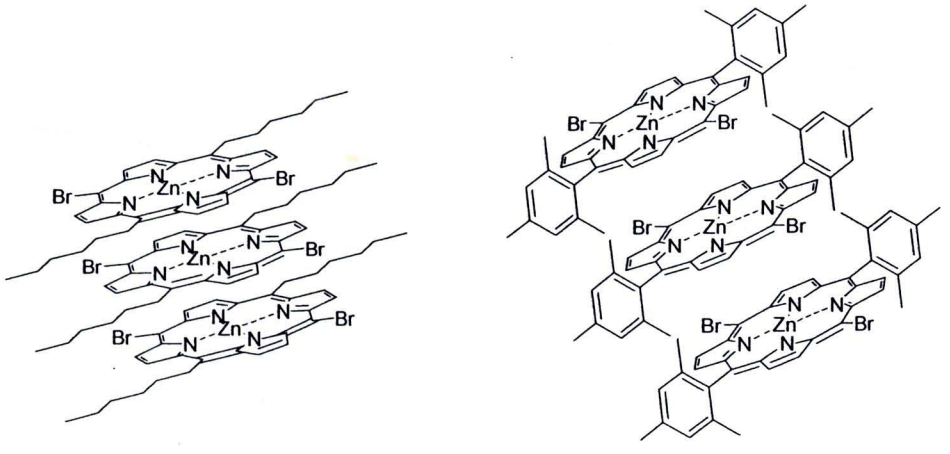

Zn-Br_2DHP Zn-Br_2DMP

Figure 3.9 The π-π stacking interactions of Zn-Br_2DHP and Zn-Br_2DMP

As a result, it can be concluded that Zn-Br_2DHP is not a good porphyrin building block, while Zn-Br_2DMP is the best candidate as porphyrin building block for the preparation of alkyne-linked porphyrin metal complexes in the next step.

3.3 Synthesis of Alkyne-Linked Porphyrin Metal Complexes

In this research, alkyne-linked porphyrin derivatives were synthesized from dibrominated porphyrin building blocks and terminal alkyne compounds by Sonogashira coupling reactions. Some terminal alkyne compounds such as trimethylsilylacetylene and phenylacetylene are commercially available, whereas

some must be prepared. All of the substituted arylethyne derivatives were prepared by the coupling reaction of aryl halides with trimethylsilylacetylene and followed by the deprotection of trimethylsilyl groups using treatments with K_2CO_3 in MeOH/Et_2O. The synthesized results of these compounds are summarized in **Table 3.6** and **Table 3.7**.

Table 3.6 Synthesis of aryltrimethylsilylethyne derivatives

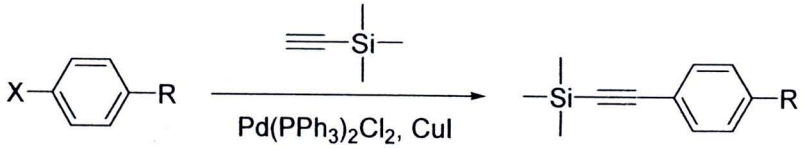

Entry	Product	X	R	Condition	Yield (%)
1	DMAP-TMSE, **3**	Br	NMe_2	PPh_3, piperidine, reflux, 12 h	62
2	NP-TMSE, **5**	Br	NO_2	Et_3N, benzene, 60 °C, 24 h	84
3	CP-TMSE, **7**	Br	CN	PPh_3, Et_3N, THF, rt, 19 h	72
4	FP-TMSE, **9**	Br	CHO	Et_3N, THF, rt, 20 h	59
5	CarP-TMSE, **11**	I	COOH	Et_3N, THF, rt, 22 h	69

Table 3.7 Synthesis of arylethyne derivatives

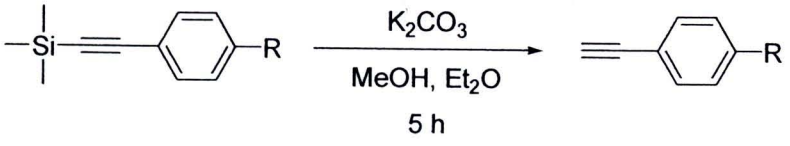

Entry	Product	R	Yield (%)
1	DMAPE, **4**	NMe_2	86
2	NPE, **6**	NO_2	93
3	CPE, **8**	CN	99
4	FPE, **10**	CHO	38
5	CarPE, **12**	COOH	83

3.3.1 Attempts to Synthesize Alkyne-Linked Porphyrin from Free Base Porphyrin

At first, attempts have been made to synthesize free base alkyne-linked porphyrin from free base dibrominated porphyrin *via* Sonogashira coupling reaction. The reaction of Br_2DHP and trimethylsilylacetylene was carried out overnight in the presence of $Pd(PPh_3)_2Cl_2$, CuI, and triethylamine in dried THF at room temperature under N_2. After a workup and purification by column chromatography, the product was obtained as a dark green solid. Characterization by MALDI-TOF mass spectrometry showed an unexpected result. As illustrated in **Figure 3.10**, the molecular ion peak at 731.425 which was consistent with calculated exact mass of Cu-$(TMSE)_2DHP$ was found as a major peak. While that of the desired $(TMSE)_2DHP$ was detected at 671.386 with very low intensity.

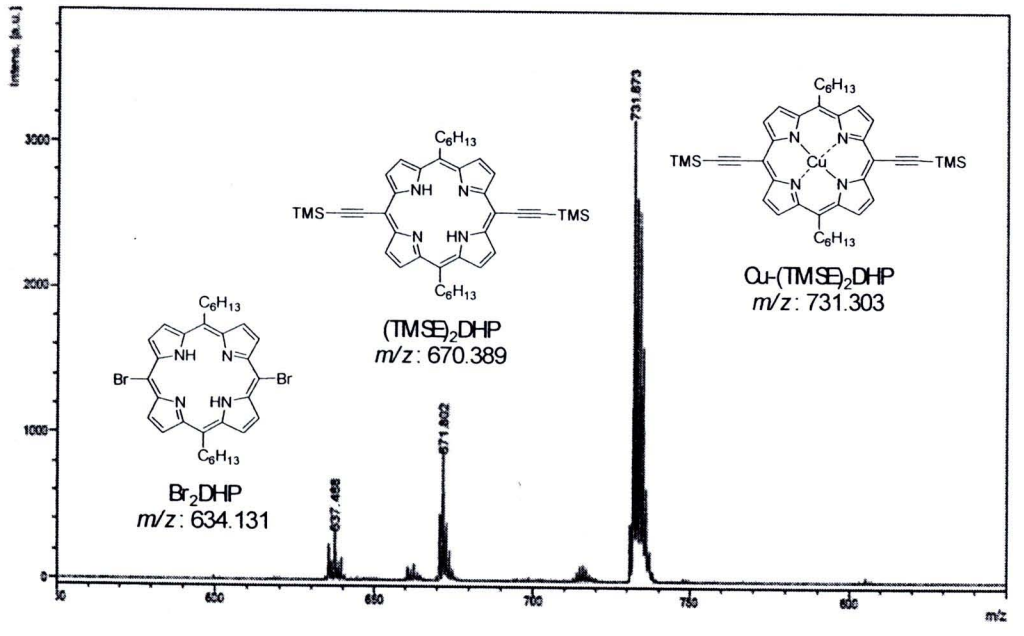

Figure 3.10 The MALDI-TOF mass spectrum of product from the reaction between Br_2DHP and trimethylsilylacetylene

The MALDI-TOF mass spectrum in **Figure 3.10** indicated the undesired insertion of Cu(I) ion from CuI into the core of porphyrin ring. It suggested that this synthetic strategy is not a good way to prepare alkyne-linked porphyrins. However, this problem can be solved by the formation of metal complexes of porphyrin building blocks before carrying out the coupling reactions.

3.3.2 Synthesis of [5,15-Bis(trimethylsilylethynyl)-10,20-dimesityl-porphyrinato]zinc(II) (Zn-(TMSE)$_2$DMP, 22)

The coupling reaction of Zn-Br$_2$DMP and trimethylsilylacetylene using Pd(PPh$_3$)$_2$Cl$_2$ as catalyst, CuI as co-catalyst, and triethylamine as base was carried out in dried THF at room temperature under N_2 for 24 hours. Under this condition, [5,15-bis(trimethylsilylethynyl)-10,20-dimesitylporphyrinato]zinc(II) (Zn-(TMSE)$_2$DMP, **22**) was gained as a dark purple solid in high yield (88%) and then characterized by ^{1}H NMR spectroscopy and MALDI-TOF mass spectrometry.

From the ^{1}H NMR spectrum of Zn-(TMSE)$_2$DMP, the β-proton signals of porphyrin ring were found at δ 8.74 and 9.63 ppm and the mesityl proton signals were found at δ 1.81, 2.64 and 7.29 ppm. Importantly, the characteristic signal of protons in trimethylsilyl groups appeared at δ 0.58 ppm. This is the best evidence to confirm the structure of Zn-(TMSE)$_2$DMP. In addition to the ^{1}H NMR data, MALDI-TOF mass spectrum was also used to confirm the formation of the product with the molecular ion peak at 801.062. This is in good agreement with calculated exact mass of Zn-(TMSE)$_2$DMP at 800.271.

3.3.3 Synthesis of (5,15-Diethynyl-10,20-dimesitylporphyrinato)zinc(II) (Zn-E$_2$DMP, 23)

The terminal alkyne zinc complex of 5,15-dimesitylporphyrin (Zn-E$_2$DMP, **23**) was prepared by the deprotection of two trimethylsilyl groups of the Zn-(TMSE)$_2$DMP with TBAF solution (1 M in THF). After 30 minutes, the reaction was quenched by an addition of water and extracted to give the product as a purple solid in 62% yield. The ^{1}H NMR spectroscopy and MALDI-TOF mass spectrometry were used to assign the structure of product.

Similar to the ^{1}H NMR spectrum of Zn-(TMSE)$_2$DMP, that of Zn-E$_2$DMP showed the β-proton signals at δ 8.77 and 9.66 ppm and the mesityl proton signals were found at δ 1.82, 2.65 and 7.30 ppm. As expected, the characteristic signal of trimethylsilyl protons at δ 0.58 ppm had disappeared and the characteristic signal of terminal alkyne protons appeared at δ 4.12 ppm. This confirmed the success of the deprotection of trimethylsilyl groups from Zn-(TMSE)$_2$DMP to obtain Zn-E$_2$DMP.

Furthermore, the molecular ion peak at 656.919 was presented in MALDI-TOF mass spectrum corresponding to calculated exact mass of Zn-E_2DMP at 656.192.

3.3.4 Synthesis of Arylethyne-Linked Porphyrin Metal Complexes

All symmetric arylethyne-linked porphyrin metal complexes consisted of Zn-(PE)$_2$DMP (**24**), Mn-(PE)$_2$DMP (**25**), Zn-(DMAPE)$_2$DMP (**27**), Zn-(NPE)$_2$DMP (**29**), Zn-(CPE)$_2$DMP (**30**), Zn-(FPE)$_2$DMP (**31**), and Zn-(CarPE)$_2$DMP (**32**) could be synthesized by the coupling reaction between Zn-Br$_2$DMP and several arylethyne derivatives under the same condition. The reactions were carried out in the presence of $Pd(PPh_3)_4$, CuI, and diisopropylamine in dried THF at 60 °C under N_2 for 24 hours. The structure and yield of the desired products are as shown in **Table 3.8**.

Table 3.8 The structure and yield of symmetric arylethyne-linked porphyrin metal complexes

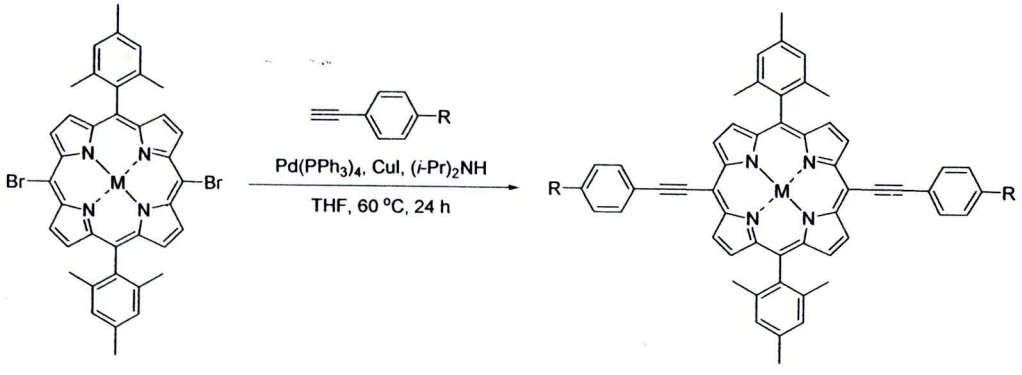

Entry	Porphyrins	M	R	Yield (%)
1	Zn-(PE)$_2$DMP, **24**	Zn	H	44
2	Mn-(PE)$_2$DMP, **25**	Mn	H	50
3	Zn-(DMAPE)$_2$DMP, **27**	Zn	NMe_2	21
4	Zn-(NPE)$_2$DMP, **29**	Zn	NO_2	50
5	Zn-(CPE)$_2$DMP, **30**	Zn	CN	40
6	Zn-(FPE)$_2$DMP, **31**	Zn	CHO	29
7	Zn-(CarPE)$_2$DMP, **32**	Zn	COOH	33

In the case of Zn-(DMAPE)(Br)DMP (**26**), it could be synthesized from the coupling reaction of Zn-Br_2DMP with 4-*N*,*N*-dimethylaminophenylethyne (DMAPE, **4**) containing $Pd(PPh_3)_4$, CuI, and diethylamine in dried THF at room temperature under N_2 for 48 hours. In order to prevent the formation of disubstituted arylethyne-linked porphyrins, 1.5 equivalents of arylethyne **4** and room temperature condition were applied in the reaction. After purification by column chromatogaphy, Zn-(DMAPE)(Br)DMP was collected as a dark green solid in moderate yield (26%). Nevertheless, the remaining unreacted porphyrin building block Zn-Br_2DMP was isolated in 33%.

Consequently, the asymmetric arylethyne-linked porphyrin derivative Zn-(DMAPE)(NPE)DMP (**28**) was synthesized from coupling 4-nitrophenylethyne (NPE, **6**) to the *meso*-bromo substituents of Zn-(DMAPE)(Br)DMP (**26**). The desired product was produced under the condition of $Pd(PPh_3)_2Cl_2$, CuI, and triethylamine in dried THF at 40 °C under N_2 for 6 days and purified by column chromatography. Pure Zn-(DMAPE)(NPE)DMP was obtained in quite a low yield (12%).

Finally, all of the synthesized arylethyne-linked porphyrin metal complexes were characterized by ^1H NMR spectroscopy and MALDI-TOF mass spectrometry. The results of characterization are as shown in **Table 3.9** and **Table 3.10**.

Table 3.9 The ^{1}H NMR chemical shifts of synthesized arylethyne-linked porphyrin metal complexes

Porphyrins	Chemical shifts		
	β-protons	mesityl protons	aryl protons
Zn-$(PE)_2$DMP, **24**[a]	8.76, 9.71	1.85, 2.66, 7.31	7.49, 7.56, 8.01
Mn-$(PE)_2$DMP, **25**[a,c]	-	-	-
Zn-(DMAPE)(Br)DMP, **26**[b]	8.43, 8.48, 9.39, 9.53	1.70, 2.52, 7.26	6.84, 7.80
Zn-$(DMAPE)_2$DMP, **27**[b]	8.50, 9.55	1.81, 2.61, 7.35	6.93, 7.87
Zn-(DMAPE)(NPE)DMP, **28**[b]	8.52, 8.57, 9.60, 9.64	1.82, 2.62, 7.36	6.93, 7.90, 8.36, 8.47
Zn-$(NPE)_2$DMP, **29**[b]	8.61, 9.71	1.82, 2.62, 7.38	8.38, 8.46
Zn-$(CPE)_2$DMP, **30**[b]	8.59, 9.69	1.81, 2.62, 7.37	8.11, 8.31
Zn-$(FPE)_2$DMP, **31**[b]	8.59, 9.69	1.81, 2.62, 7.37	8.10, 8.31
Zn-$(CarPE)_2$DMP, **32**[b]	8.57, 9.64	1.81, 2.62, 7.36	8.12, 8.19

[a] measured in $CDCl_3$
[b] measured in DMSO-d_6
[c] The ^{1}H NMR spectrum of Mn-$(PE)_2$DMP was difficult to identify.

Table 3.10 The MALDI-TOF mass data of synthesized arylethyne-linked porphyrin metal complexes

Porphyrins	Calculated exact mass	Molecular ion peak
Zn-$(PE)_2$DMP, **24**	808.254	809.232
Mn-$(PE)_2$DMP, **25**	799.263	799.896
Zn-(DMAPE)(Br)DMP, **26**	829.176	832.157
Zn-$(DMAPE)_2$DMP, **27**	894.339	895.298
Zn-(DMAPE)(NPE)DMP, **28**	896.282	897.084
Zn-$(NPE)_2$DMP, **29**	898.225	899.349
Zn-$(CPE)_2$DMP, **30**	858.245	859.070
Zn-$(FPE)_2$DMP, **31**	864.244	865.152
Zn-$(CarPE)_2$DMP, **32**	896.234	897.398

3.4 Investigation of Photophysical Properties

It is well known that porphyrins are tetrapyrrolic macrocycles which have an extensive system of delocalized π-electrons on the carbon-nitrogen framework. Because of the large π-conjugated system, porphyrins exhibit extraordinary photophysical properties that are useful for several applications. These properties can be tuned by changing the central metal ions, connecting with different peripheral substituents, coordinating with axial ligands, or expanding the macrocycle sizes.

In this research, photophysical properties of all synthesized porphyrins were investigated by UV-visible absorption spectroscopy and fluorescence emission spectroscopy. Furthermore, effects of metal ions and various substituents on these properties were also discussed.

3.4.1 UV-Visible Spectroscopy

The UV-visible absorption spectra of all synthesized porphyrins were measured at a 10^{-5} M concentration in THF solution. The absorption maxima at both Soret band and Q bands of the solutions of porphyrins are summarized in **Table 3.11**. Moreover, the visual color of the solutions of porphyrins at a 10^{-4} M concentration in THF was observed as illustrated in **Figure 3.11**.

From **Table 3.11** and **Figure 3.11**, it can be observed that the visual color of the solutions of porphyrins was relative to the absorption properties based on the general visual color theory. For example, DHP, Zn-DHP, DMP, and Zn-DMP exhibited the color of the solutions in red tone which was consistent with the absorption at shorter wavelength. On the other hand, alkyne-linked and arylethyne-linked porphyrins displayed green solutions resulting from the absorption maxima in red region. More importantly, these results indicated that central metal ions and some substituents on porphyrin rings influenced the electronic absorption properties of porphyrins which were described as follows.

Table 3.11 Absorption maxima of the solutions of all synthesized porphyrins at a 10^{-5} M concentration in THF

porphyrins	absorption maxima (λ_{max}, nm)	
	Soret bands	Q bands
DHP, **13**	402	502 533 578 634
Zn-DHP, **14**	410	546 578
Br_2-DHP, **15**	418	522 555 605 665
Zn-Br_2DHP, **16**	427	568 614
DMP, **17**	404	500 531 575 630
Zn-DMP, **18**	410	544 578
Mn-DMP, **19**	422 460	561
Zn-Br_2DMP, **20**	427	566 606
Mn-Br_2DMP, **21**	410 488	647
Zn-$(TMSE)_2$DMP, **22**	438 446	582 634
Zn-E_2DMP, **23**	432 441	573 624
Zn-$(PE)_2$DMP, **24**	447	597 651
Mn-$(PE)_2$DMP, **25**	445 489	675
Zn-(DMAPE)(Br)DMP, **26**	452	585 643
Zn-$(DMAPE)_2$DMP, **27**	467	676
Zn-(DMAPE)(NPE)DMP, **28**	456	583 678
Zn-$(NPE)_2$DMP, **29**	461	579 668
Zn-$(CPE)_2$DMP, **30**	453	583 660
Zn-$(FPE)_2$DMP, **31**	455	588 663
Zn-$(CarPE)_2$DMP, **32**	451	583 658

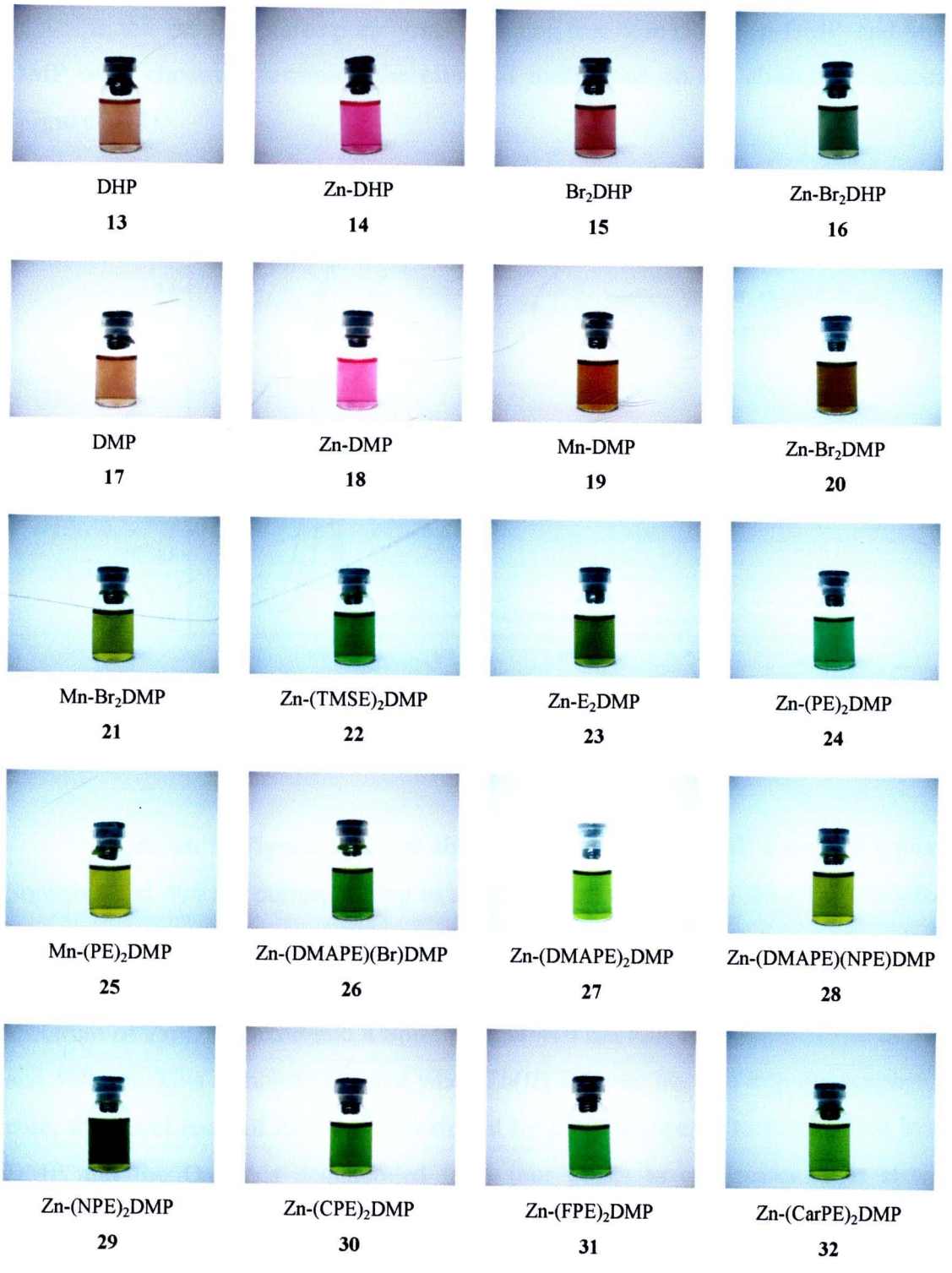

Figure 3.11 The visual color of the solutions of porphyrins at a 10^{-4} M concentration in THF

3.4.1.1 Effect of Metal Ions

In this research, three porphyrins including free base DMP, Zn-DMP, and Mn-DMP were chosen to examine the effect of metal ions on the absorption spectra (**Figure 3.12**).

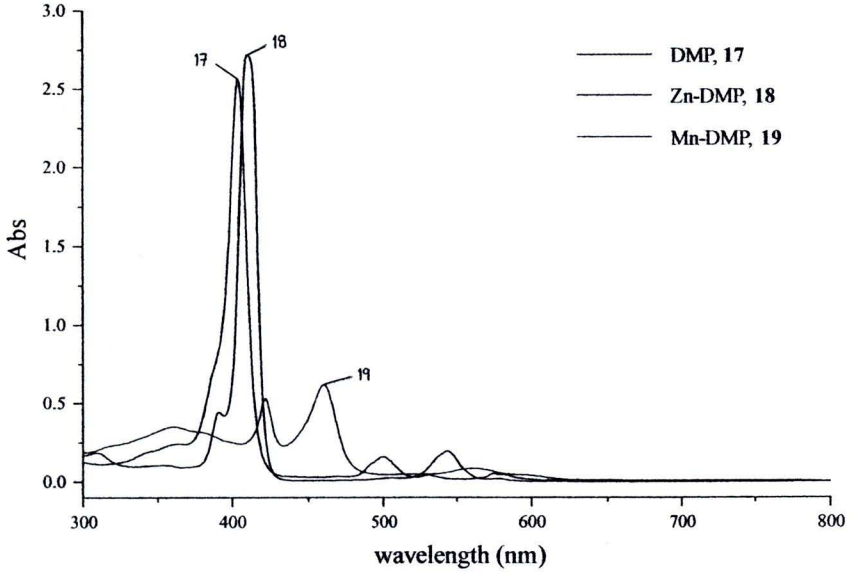

Figure 3.12 UV-visible absorption spectra of DMP, Zn-DMP, and Mn-DMP

As shown in **Figure 3.12**, the absorption spectrum of DMP showed a typical Soret band at 404 nm corresponding to a strong π-π^* transition to the second excited ($S_0 \rightarrow S_2$) and four Q bands at 500, 531, 575, and 630 nm corresponding to a weak π-π^* transition to the first excited ($S_0 \rightarrow S_1$), respectively [39]. In contrast, the absorption spectrum of Zn-DMP exhibited a Soret band at 410 nm and only two Q bands at 544 and 578 nm. This demonstrated that when Zn(II) ion was inserted into the porphyrin core, the Soret band of Zn-DMP red shifted by 6 nm compared to that of free base DMP and the Q bands degenerated from four peaks to two peaks. This is the characteristic properties of porphyrin zinc complexes [63,64] which can be explained by the average electron density of the porphyrin ring and the symmetry of the molecule [65].

In general, the central part of the metalloporphyrin ring is occupied by a metal ion linked to a pyrrole ring. The metal ion accepts the lone pair electrons of the nitrogen atoms of the pyrrole ring, while electrons of the metal ion can be donated back to the porphyrin ring leading to the formation of delocalized π-bonds which

permit the easy flow of electrons within the delocalized π-system. Based on this concept, the delocalized π-bonds of porphyrin zinc complexes, including Zn-DMP, increased the average electron density of the porphyrin ring and decreased the energy available for electronic transition. As a result, a red shift in the Soret band is observed. In the case of the degeneration of the Q bands, it can be elucidated relying on the fact that when the metal ion coordinates with the nitrogen atoms of porphyrin ring, the symmetry of the molecular increases and the number of Q bands, therefore, decreases [40,66].

In addition, a UV-visible absorption spectrum of Mn-DMP was also obtained. It showed two Soret bands at 422 and 460 nm which red shifted largely compared to that of DMP and Zn-DMP, a weak Q band at 561 nm, and a broad absorption band at 300 to 400 nm. This spectroscopic result of Mn-DMP is similar to that of the general porphyrin manganese complexes which was reported previously such as (*meso*-tetraphenylporphyrinato)manganese(II) [64] and (5-hydroxyphenyl-10,15,20-triphenylporphyrinato)manganese(II) [40]. The red shifts of Soret bands and the degeneration of Q bands in the absorption spectrum of Mn-DMP can be explained by the same reason as that of Zn-DMP.

3.4.1.2 Effect of Hexyl and Mesityl Side Chains

To study the effect of hexyl and mesityl side chains in porphyrin building blocks on the electronic absorption property, the absorption spectra of two series of porphyrin building blocks were compared as illustrated in **Figure 3.13**. A series of dihexylporphyrin derivatives consists of free base DHP, Zn-DHP, and Zn-Br_2DHP, while a series of dimesitylporphyrin derivatives consists of free base DMP, Zn-DMP, and Zn-Br_2DMP.

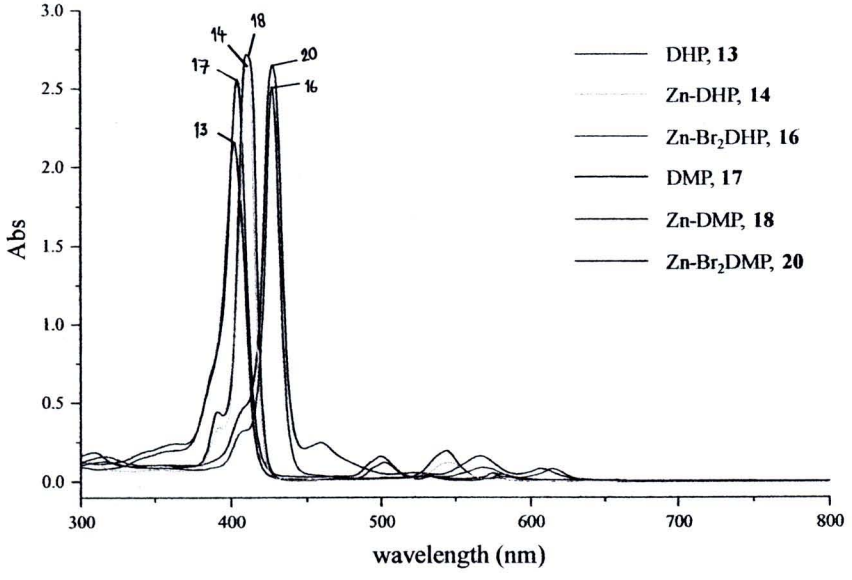

Figure 3.13 UV-visible absorption spectra of DHP, Zn-DHP, Zn-Br_2DHP, DMP, Zn-DMP, and Zn-Br_2DMP

From **Figure 3.13**, all of the absorption spectra of dihexylporphyrin derivatives (DHP, Zn-DHP, and Zn-Br_2DHP) displayed Soret band and Q bands in a similar manner to those of dimesitylporphyrin derivatives (DMP, Zn-DMP, and Zn-Br_2DMP). The absorption maxima of each porphyrin in this observation are listed in **Table 3.11**. As shown, DHP showed absorption maxima in the same range as DMP. Likewise, Zn-DHP gave an absorption pattern with absorption maxima which is closely resembling to its dimesityl counterpart, Zn-DMP. Similarly, the dibrominated derivative pair, Zn-Br_2DHP and Zn-Br_2DMP, exhibited relatively similar electronic absorptions. This indicated that both hexyl and mesityl side chains do not possess adequate ability to perturb the electronic structure of porphyrins. Due to the fact that the hexyl group is not conjugating substituent, it cannot extend the π-conjugated system of porphyrins. In the case of the mesityl group, although delocalized π-electrons are present in the aromatic ring, there is minimal π-overlap between the π-conjugated system of the porphyrin ring and that of the mesityl aryl ring. They basically exist as isolated conjugating systems. This non-conjugating behavior can be attributed to the large aryl-porphyrin dihedral angles which result from the steric interactions between the β-hydrogens of porphyrin ring and the *ortho*-substituents on the aryl rings. To support this assumption, the distribution of aryl-porphyrin dihedral

angles for some *ortho*-unsubstituted, *β*-unsubstituted *meso*-aryl porphyrins from the Cambridge Crystallographic Database (CCD) [67] is illustrated in **Figure 3.14**.

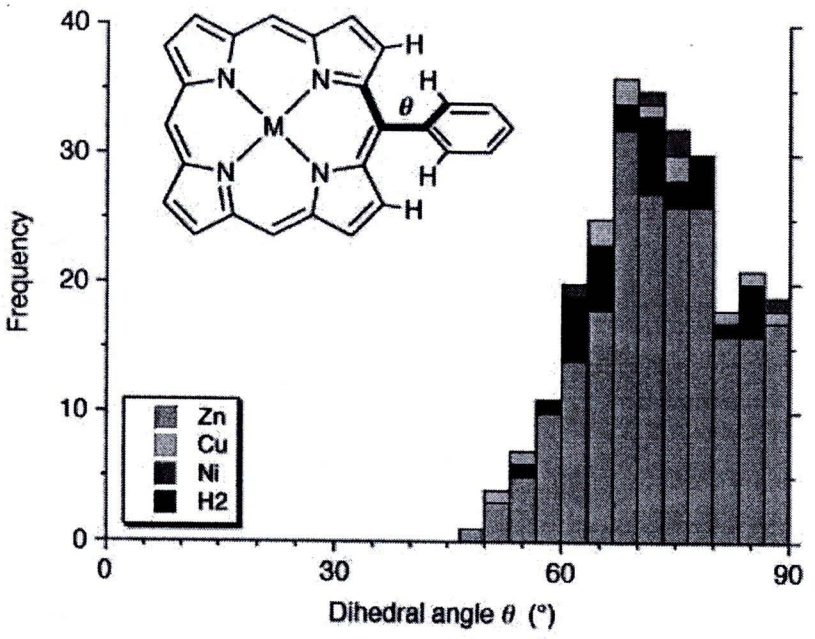

Figure 3.14 The distribution of dihedral angles in *meso*-aryl Zn(II), Cu(II), Ni(II), and free base porphyrins from the CCD [67]

In other words, it can be concluded that non-conjugated and conjugated substituents which are not able to allow planar π-overlap with porphyrin ring cannot affect the electronic structure of porphyrins. Consequently, their absorption spectra are almost identical to those of unsubstituted porphyrins.

3.4.1.3 Effect of Bromo Substituents

A comparison between the absorption spectrum of dibrominated porphyrin Zn-Br_2DMP and that of the corresponding porphyrin Zn-DMP is exhibited in **Figure 3.13**. The absorption spectrum of Zn-DMP showed a Soret band at 410 nm and two Q bands at 544 and 578 nm, while the spectrum of Zn-Br_2DMP showed a Soret band at 427 nm which has obviously red shifted by about 17 nm and two Q bands at 566 and 606 nm which has remarkably red shifted compared to that of Zn-DMP.

In addition, similar results were observed in when comparing the absorption spectra of Br_2DHP and Zn-Br_2DHP with those of corresponding porphyrins DHP and Zn-DHP, respectively as exhibited in **Figure 3.15**.

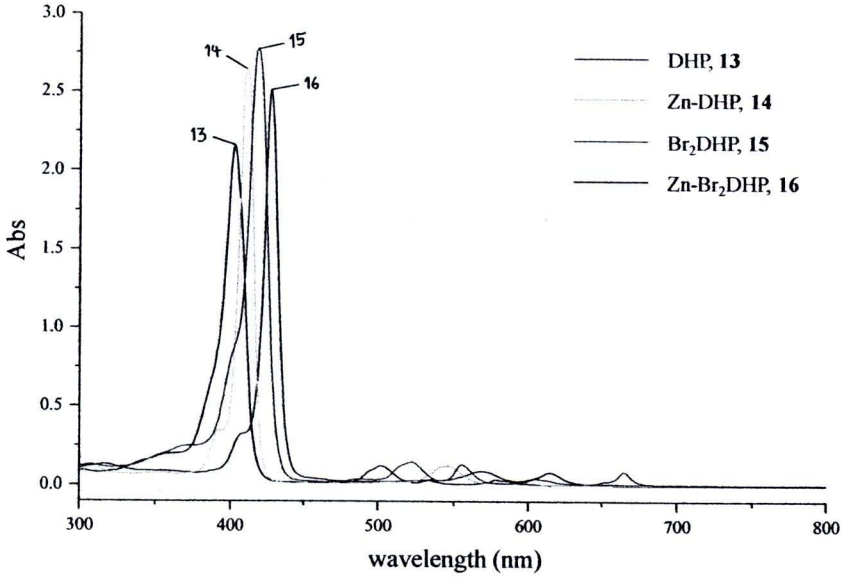

Figure 3.15 UV-visible absorption spectra of DHP, Zn-DHP, Br_2DHP, and Zn-Br_2DHP

These observations confirmed that bromo substituents attached to the *meso*-positions of both free base porphyrins and porphyrin zinc complexes influenced the absorption behavior of the compounds. A possible explanation is that bromo substituents have non-bonding electrons which can delocalize into the porphyrin ring leading to the change in the electronic structure of molecules and result in the significant red shifts in the absorption spectra.

3.4.1.4 Effect of Alkyne Linkers

To investigate the effect of alkyne linkers on the electronic absorption spectra of the porphyrin systems, the absorption spectra of alkyne-linked porphyrins Zn-$(TMSE)_2$DMP and Zn-E_2DMP were compared to the absorption spectrum of Zn-DMP as depicted in **Figure 3.16**.

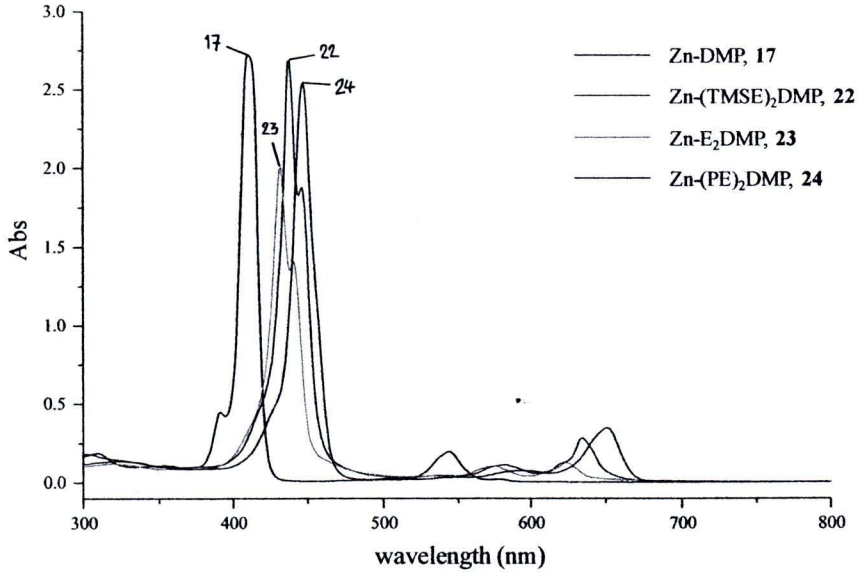

Figure 3.16 UV-visible absorption spectra of Zn-DMP, Zn-$(TMSE)_2$DMP, Zn-E_2DMP, and Zn-$(PE)_2$DMP

In the case of Zn-$(TMSE)_2$DMP, the absorption spectrum showed split Soret bands at 438 and 446 nm and intensified Q bands at 582 and 634 nm. Similarly, the absorption spectrum of Zn-E_2DMP showed split Soret bands at 432 and 441 nm and intensified Q bands at 573 and 624 nm which has slightly blue shifted relative to those of Zn-$(TMSE)_2$DMP.

Both Soret bands and Q bands of Zn-$(TMSE)_2$DMP and Zn-E_2DMP presented clearly red shifts compared to those of Zn-DMP. The surprising splitting of Soret bands and the clearly red shifts in both Soret bands and Q bands are evidences which confirm the extension of π-conjugated system [68,69]. In fact, higher conjugation causes splitting in the π and π^* levels which results in a reduced HOMO-LUMO gap. Hence, the simplest manifestations of this are red shifts and broadening in the electronic spectra [39]. Based on this fact, it can be concluded that alkyne linkers can allow planar π-overlap with porphyrin ring and may be able to exhibit strong electronic communications between them.

3.4.1.5 Effect of Arylethyne Linkers

In order to extend the π-conjugated systems of alkyne-linked porphyrins, phenyl and several other aryl derivatives containing different substituents were connected to the other side of the alkyne linkers. Owing to the fact that alkyne linkers are useful for keeping the porphyrins coplanar and maximizing the π-overlap, it was anticipated that arylethyne-linked porphyrins would display the extraordinary photophysical properties.

As expected, the absorption spectrum of phenylethyne-linked porphyrin Zn-$(PE)_2$DMP exhibited a broad Soret band at 447 nm which has clearly red shifted compared to that of Zn-DMP at 410 nm and that of Zn-E_2DMP at 432 and 441 nm. Furthermore, The Q bands of Zn-$(PE)_2$DMP appeared at 597 and 651 nm which were also red shifted and intensified compared to those of Zn-DMP and Zn-E_2DMP (**Figure 3.16**).

In the case of arylethyne-linked porphyrins, the absorption spectra of all synthesized symmetric arylethyne-linked porphyrins including Zn-$(DMAPE)_2$DMP, Zn-$(NPE)_2$DMP, Zn-$(CPE)_2$DMP, Zn-$(FPE)_2$DMP, and Zn-$(CarPE)_2$DMP relative to the spectrum of Zn-$(PE)_2$DMP are exhibited in **Figure 3.17**.

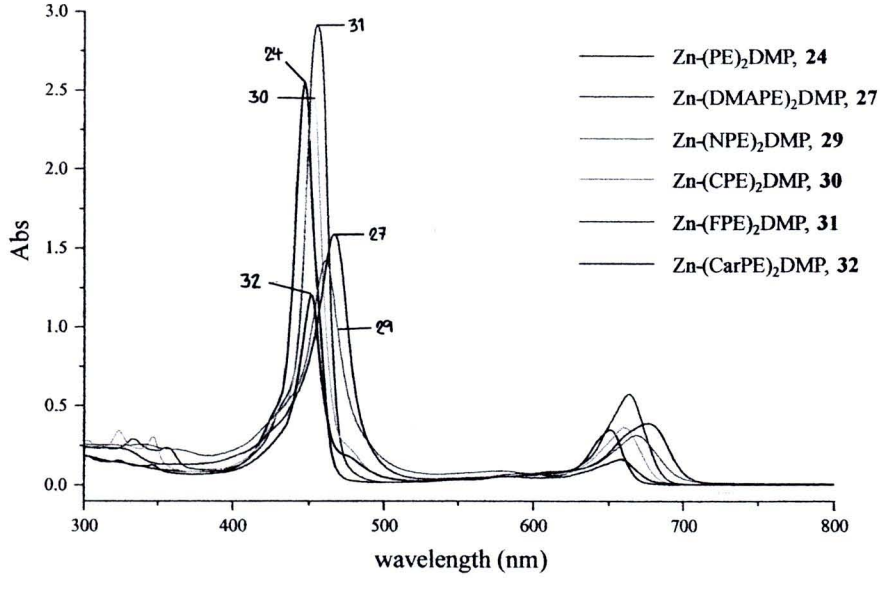

Figure 3.17 UV-visible absorption spectra of Zn-$(PE)_2$DMP, Zn-$(DMAPE)_2$DMP, Zn-$(NPE)_2$DMP, Zn-$(CPE)_2$DMP, Zn-$(FPE)_2$DMP, and Zn-$(CarPE)_2$DMP

From **Figure 3.17**, the absorption spectra of all symmetric arylethyne-linked porphyrins showed red shifted Soret band and Q bands corresponding to those of Zn-$(PE)_2$DMP. These results revealed that the substituents which possess π-electrons or π-orbitals could affect the electronic structure of porphyrins by extending the π-conjugated length. Among all arylethyne-linked porphyrins, the red shifts in their absorption spectra decrease in the following order: Zn-$(DMAPE)_2$DMP > Zn-$(NPE)_2$DMP > Zn-$(FPE)_2$DMP > Zn-$(CPE)_2$DMP > Zn-$(CarPE)_2$DMP. The main reason for this order may be because of their abilities to conjugate with the π-conjugated systems of porphyrins.

Interestingly, Zn-$(DMAPE)_2$DMP exhibited the largest red shifts in both Soret band and Q band at 467 and 676 nm, respectively. This finding can be implied that the *N*,*N*-dimethylamino substituent, as an electron donating group, induced stronger perturbation of the electronic structure of porphyrins than that of other substituents which are electron withdrawing groups. Similar to the effect of Zn(II) ion, it may be explained by an increase in average electron density of the porphyrin which lead to a decrease in the energy gap responsible for electronic transitions involved.

In addition, the absorption spectra of asymmetric arylethyne-linked porphyrins such as Zn-(DMAPE)(Br)DMP and Zn-(DMAPE)(NPE)DMP were investigated as shown in **Figure 3.18**.

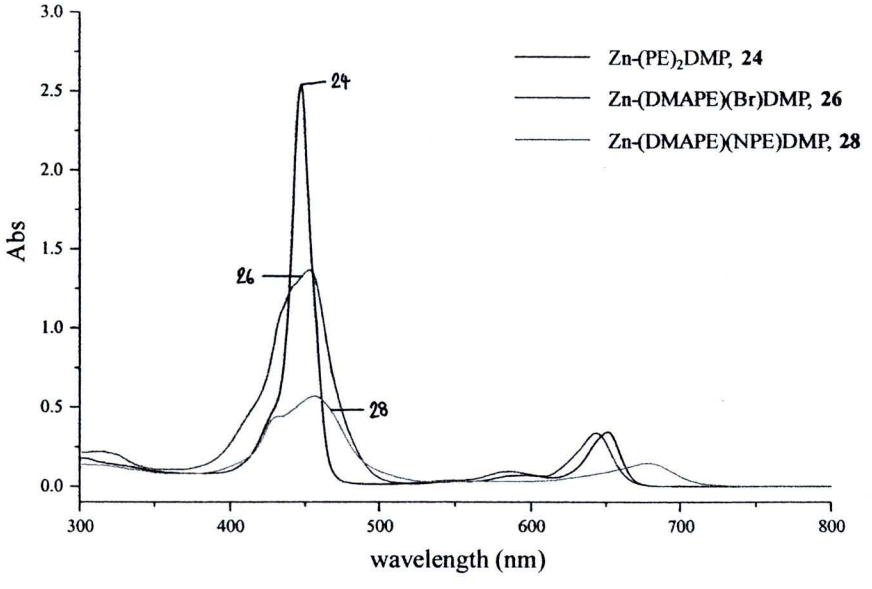

Figure 3.18 UV-visible absorption spectra of Zn-$(PE)_2$DMP, Zn-(DMAPE)(Br)DMP and Zn-(DMAPE)(NPE)DMP

The absorption spectrum of Zn-(DMAPE)(Br)DMP showed a broad Soret band at 542 nm and Q bands at 585 and 643 nm. Surprisingly, the Soret band of Zn-(DMAPE)(Br)DMP, which possesses only one arylethyne moiety, was found at a wavelength relatively close to that of Zn-$(CPE)_2$DMP (453 nm), Zn-$(FPE)_2$DMP (455 nm), and Zn-$(CarPE)_2$DMP (451 nm), which possess two aryethyne moities. This is a good result to confirm the strong effect of the *N*,*N*-dimethylamino group on the electronic structure of porphyrins.

In the case of Zn-(DMAPE)(NPE)DMP, the absorption spectrum exhibited a broad Soret band at 456 nm which is blue shifted and Q bands at 583 and 678 nm which is red shifted compared to those of both Zn-$(DMAPE)_2$DMP and Zn-$(NPE)_2$DMP. Although this result cannot be explained clearly, it can be implied that there are some changes in the electronic structure or in the electronic transition process.

On account of the outstanding absorption properties and the large π-conjugated systems, synthesized alkyne-linked porphyrin metal complexes may find utility as photosensitized dyes in photovoltaic cells, organic semiconductors, molecular wires, and photodynamic therapeutic agents.

3.4.2 Fluorescence Spectroscopy

The fluorescence emission spectra of all synthesized porphyrins were measured at a 10^{-5} M concentration in THF solution. The excitation and emission wavelength of porphyrins are listed in **Table 3.12**. Furthermore, the fluorescence images of each porphyrin at a 10^{-4} M concentration in THF under the excitation wavelength at 366 nm are illustrated in **Figure 3.19**.

From **Table 3.12** and **Figure 3.19**, most of the synthesized porphyrins exhibited the red fluorescence emission which was consistent with the emission wavelength ranging from 630 to 750 nm. However, some of the synthesized porphyrins, particularly brominated porphyrins and porphyrin manganese complexes, did not show the fluorescence emission. These fluorescence spectroscopic data revealed that metal ions in the core of porphyrin rings and some substituents affected the fluorescence emission properties of porphyrins which were described as follows.

Table 3.12 The excitation and emission wavelength of the solutions of all synthesized porphyrins at a 10^{-5} M concentration in THF

porphyrins	excitation wavelength[a] (λ_{ex}, nm)	emission wavelength (λ_{em}, nm)
DHP, **13**	392	637 704
Zn-DHP, **14**	404	591 638
Br_2-DHP, **15**	392	-[b]
Zn-Br_2DHP, **16**	282	-[b]
DMP, **17**	396	633 700
Zn-DMP, **18**	404	584 636
Mn-DMP, **19**	262	-[b]
Zn-Br_2DMP, **20**	262	-[b]
Mn-Br_2DMP, **21**	262	-[b]
Zn-$(TMSE)_2$DMP, **22**	450	642 702
Zn-E_2DMP, **23**	444	630 687
Zn-$(PE)_2$DMP, **24**	650	660 720
Mn-$(PE)_2$DMP, **25**	260	-[b]
Zn-(DMAPE)(Br)DMP, **26**	454	-[b]
Zn-$(DMAPE)_2$DMP, **27**	680	695
Zn-(DMAPE)(NPE)DMP, **28**	682	705
Zn-$(NPE)_2$DMP, **29**	670	687 751
Zn-$(CPE)_2$DMP, **30**	662	673 733
Zn-$(FPE)_2$DMP, **31**	664	678 737
Zn-$(CarPE)_2$DMP, **32**	452	668 727

[a] the excitation wavelength for each porphyrin was obtained from the pre-scan experiments.
[b] no fluorescence emission

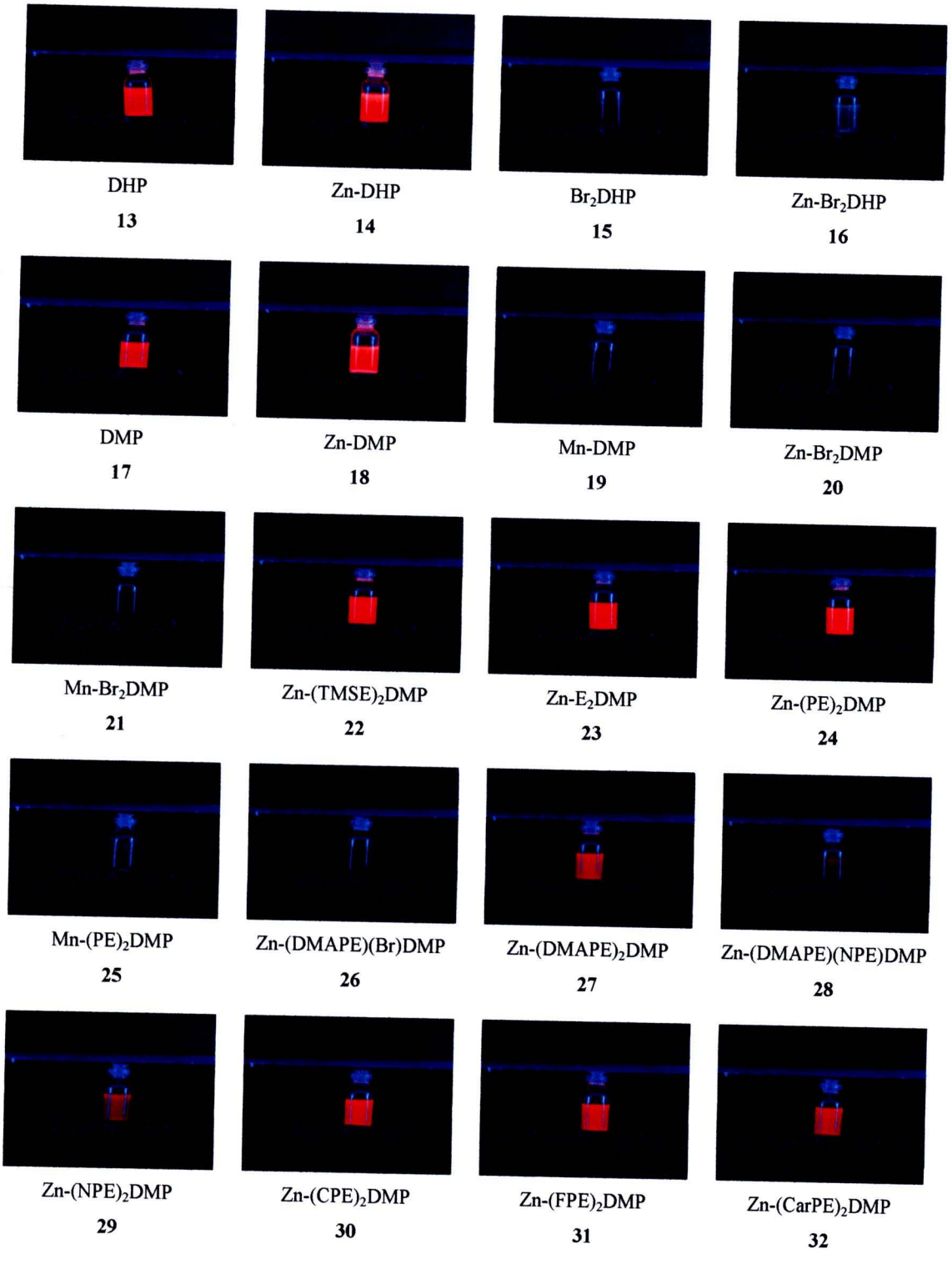

Figure 3.19 Florescence images of the solutions of porphyrins at a 10^{-4} M concentration in THF under the excitation wavelength at 366 nm

3.4.2.1 Effect of Metal Ions

In order to investigate the effect of metal ions on the emission properties of porphyrins, fluorescence emission spectra of free base DMP, Zn-DMP, and Mn-DMP were observed as shown in **Figure 3.20**.

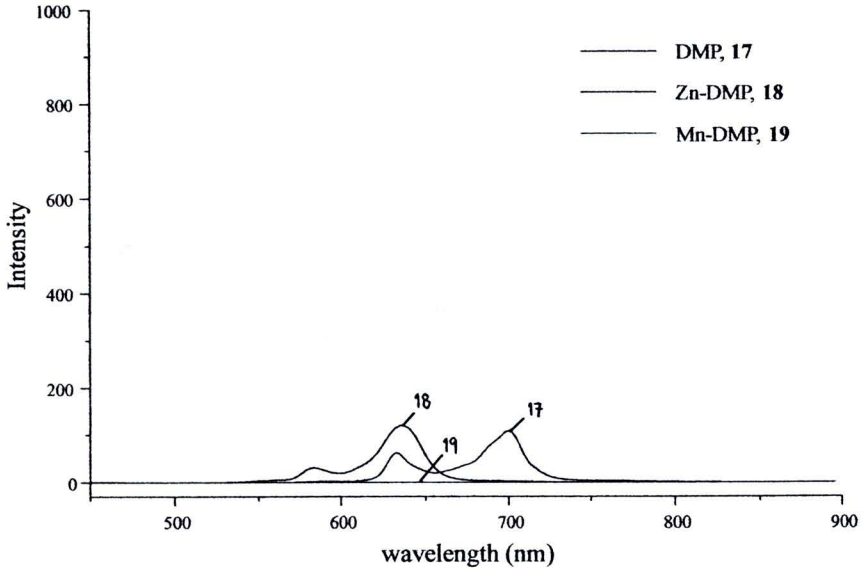

Figure 3.20 Fluorescence emission spectra of DMP, Zn-DMP, and Mn-DMP

It can be seen that the emission spectrum of free base DMP displayed two fluorescence emission peaks at 633 and 700 nm, whereas that of Zn-DMP exhibited two emission peaks at 584 and 636 nm which were blue shifted by 49 and 64 nm compared to those of DMP. A possible reason for this result is that the incorporation of Zn(II) ion has resulted in a higher symmetry of the porphyrin and the LUMO energy level has increased resulting in the observation of the blue shifts in the emission spectra [66]. Moreover, Zn(II) ion may have a small electronic interaction with the porphyrin ring. As a result, the excited state energy of the porphyrin zinc complex cannot be released by the energy transfer from the porphyrin to the metal ion. Therefore, the relaxation of the excited energy is carried out by the fluorescence emission [66].

In the case of Mn-DMP, there was no obvious emission band in the emission spectra. This is because of a strong electronic interaction between porphyrin and Mn(II) ion. After excitation with light, the excited energy of porphyrin manganese complexes can be transferred from the porphyrin to Mn(II) ion without exhibiting

fluorescence emission [66]. This assumption can be confirmed by the absence of fluorescence emission in Mn-Br_2DMP and Mn-$(PE)_2$DMP measurements.

3.4.2.2 Effect of Hexyl and Mesityl Side Chains

The fluorescence emission spectra of DHP and Zn-DHP which are dihexylporphyrin derivatives and those of DMP and Zn-DMP which are dimesitylporphyrin derivatives were compared as depicted in **Figure 3.21**.

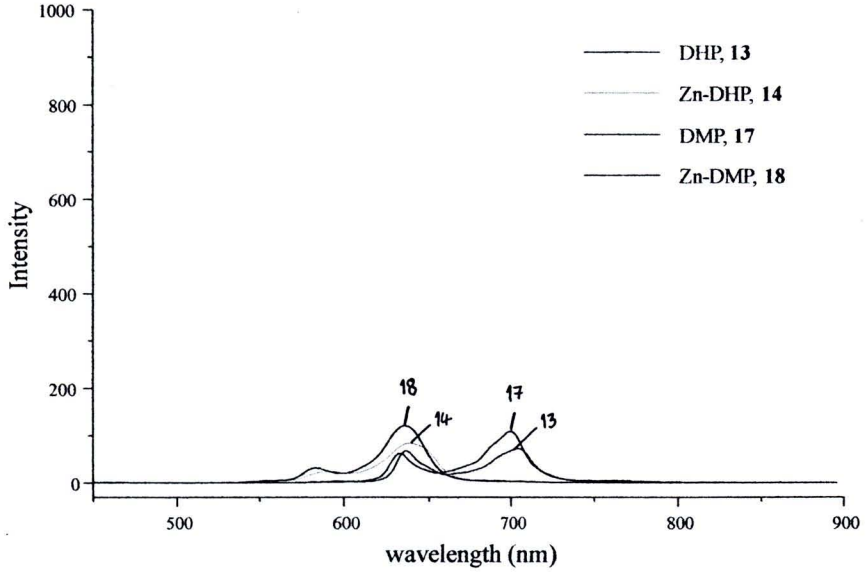

Figure 3.21 Fluorescence emission spectra of DHP, Zn-DHP, DMP, and Zn-DMP

Similar to the absorption measurements, there was no significant difference between the emission spectra of dihexylporphyrin derivatives and those of dimesitylporphyrin derivatives because both hexyl and mesityl groups could not perturb the electronic structure of porphyrins. However, the emission spectra of DHP and Zn-DHP were slightly red shifted relative to those of corresponding DMP and Zn-DMP, respectively.

3.4.2.3 Effect of Bromo Substituents

To determine the effect of bromo substituents on the fluorescence emission behavior, the emission spectra of three brominated porphyrins were measured compared to the emission spectrum of basic porphyrin Zn-DMP as shown in **Figure**

3.22. Three brominated porphyrins used in this study consist of Br_2DHP as brominated free base porphyrin, Zn-Br_2DMP as dibrominated porphyrin zinc complex, and Zn-(DMAPE)(Br)DMP as monobrominated porphyrin zinc complex.

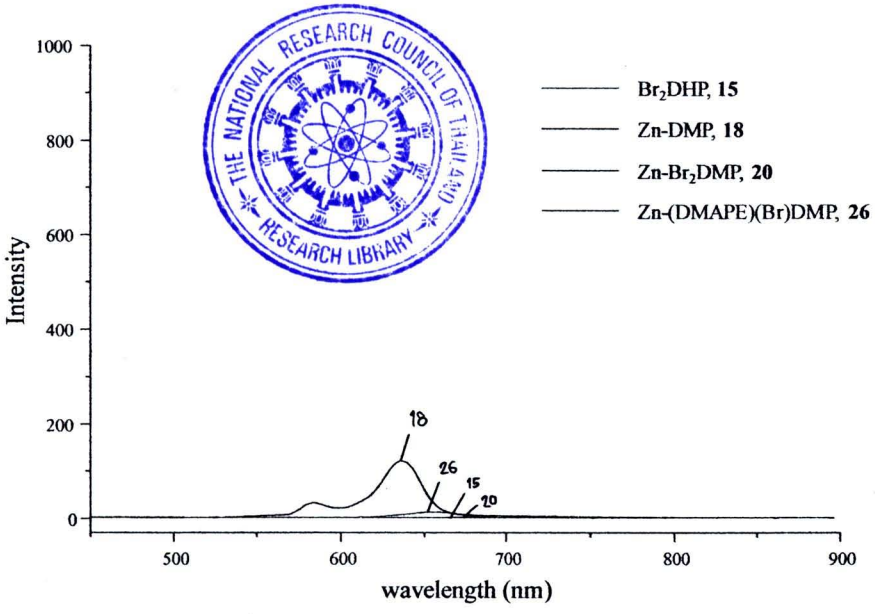

Figure 3.22 Fluorescence emission spectra of Br_2DHP, Zn-DMP, Zn-Br_2DMP and Zn-(DMAPE)(Br)DMP

Surprisingly, all brominated porphyrins did not give the fluorescence emission. This complete fluorescence quenching may be explained by the photoinduced electron transfer (PET) process (**Figure 3.23**). The PET process can occur if at least one of the non-bonding molecular orbitals of the bromo substituents has an energy level between the energy levels of the HOMO and the LUMO of the porphyrin. In other words, this can take place if the bromo substituents have at least one molecular orbital of non-bonding electrons situated between the HOMO and the LUMO of porphyrin. After exciting one electron from the HOMO to the LUMO of porphyrin by light, electron from non-bonding molecular orbital of bromo substituents can transfer to the empty HOMO of porphyrin and interrupt the relaxation from the LUMO to the HOMO. As a result, the fluorescence emission of porphyrins is quenched completely.

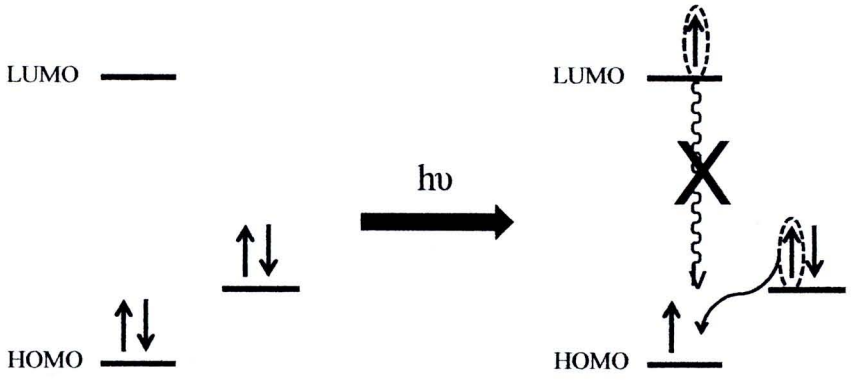

Figure 3.23 The photoinduced electron transfer (PET) process

3.4.2.4 Effect of Alkyne Linkers

The fluorescence emission spectra of Zn-(TMSE)$_2$DMP and Zn-E$_2$DMP were compared to the emission spectrum of Zn-DMP in order to examine the effect of alkyne linkers on the fluorescence emission properties (**Figure 3.24**).

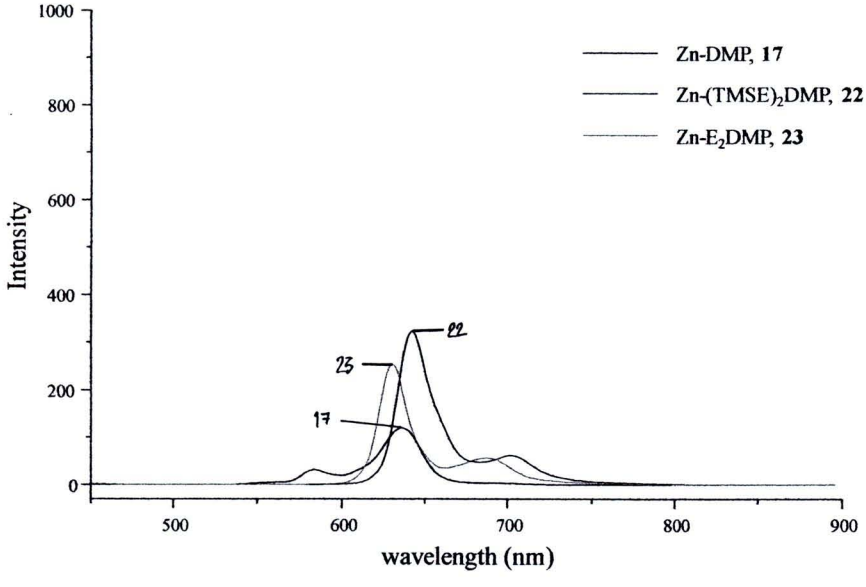

Figure 3.24 Fluorescence emission spectra of Zn-DMP, Zn-(TMSE)$_2$DMP, and Zn-E$_2$DMP

As shown in **Figure 3.24**, the fluorescence emission of Zn-(TMSE)$_2$DMP was observed a 642 and 702 nm, while that of Zn-E$_2$DMP was found at 630 and 687 nm. The fluorescence emission spectra of both Zn-(TMSE)$_2$DMP and Zn-E$_2$DMP clearly

displayed a red shift and largely intensified emission bands relative to the emission spectrum of Zn-DMP. This is in good agreement with the absorption measurements, features of which were more pronounced as the π-conjugation was extended.

3.4.2.5 Effect of Arylethyne Linkers

The fluorescence emission spectra of all arylethyne-linked porphyrin zinc complexes are presented in **Figure 3.25**. The order of the fluorescence emission maxima of these porphyrins was Zn-(DMAPE)(NPE)DMP > Zn-$(DMAPE)_2$DMP > Zn-$(NPE)_2$DMP > Zn-$(FPE)_2$DMP > Zn-$(CPE)_2$DMP > Zn-$(CarPE)_2$DMP > Zn-$(PE)_2$DMP. This order was consistent with that of the absorption maxima at Soret bands as described before. It confirmed the effect of each functional group on the electronic structure of porphyrins.

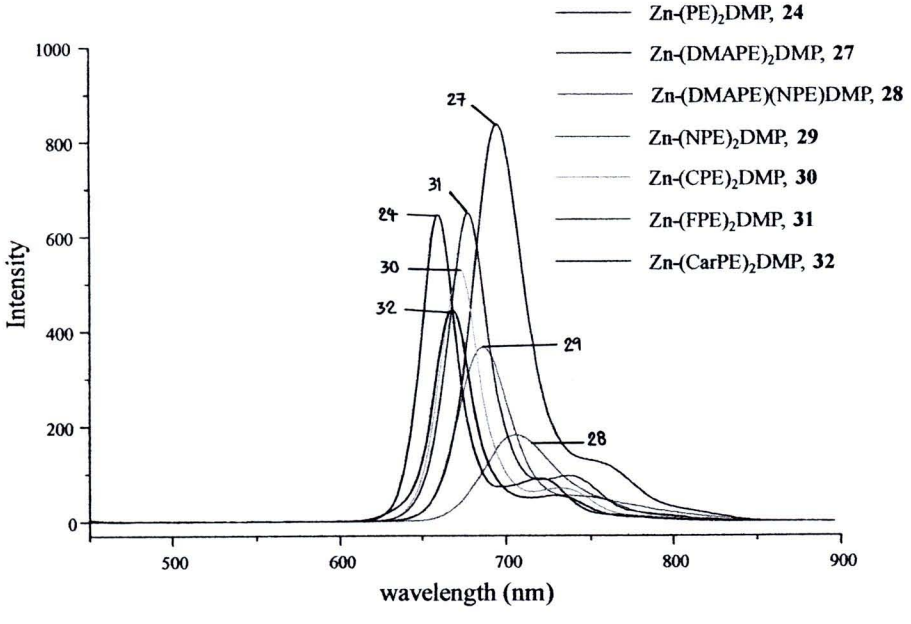

Figure 3.25 Fluorescence emission spectra of Zn-$(PE)_2$DMP, Zn-$(DMAPE)_2$DMP, Zn-(DMAPE)(NPE)DMP, Zn-$(NPE)_2$DMP, Zn-$(CPE)_2$DMP, Zn-$(FPE)_2$DMP, and Zn-$(CarPE)_2$DMP

The red shifts in the emission spectra of arylethyne-linked porphyrins compared to the emission spectrum of Zn-DMP can be accounted for by the higher π-conjugated system of porphyrins. Among all arylethyne-linked porphyrins, Zn-

$(DMAPE)_2DMP$ which possesses electron donating groups showed the highest intensity of fluorescence. On the other hand, Zn-$(NPE)_2DMP$, Zn-$(CPE)_2DMP$, Zn-$(FPE)_2DMP$, and Zn-$(CarPE)_2DMP$ which possess electron withdrawing groups exhibited lower intensity.

The fluorescence spectroscopic data suggested that alkyne-linked porphyrin zinc complexes can be strong candidates for novel fluorescence dyes or materials for lasers and organic light emitting diodes (OLEDs).

3.5 Investigation of Coordination Properties

Based on the basis of coordination properties, porphyrins have been widely investigated to utilize as basic materials in chemical sensors, especially for volatile organic compounds [70-72]. Moreover, the coordinated porphyrins are well known to exhibit special properties which are suitable for many fields including artificial photosynthesis systems [73], molecular switches [12], and nonlinear optical (NLO) materials [74-75].

Because of these interesting applications, the preliminary experiments for the investigation of coordination properties of synthesized porphyrins were carried out by ^1H NMR, UV-visible, and fluorescence spectroscopic titration. Basically, these investigations have shed light on the manner by which axial ligands induce changes in the photophysical features of porphyrins. Pyridine was chosen as a ligand in these studies because it possesses a good donor atom, simple and rigid structure without steric bulky groups which may be able to promote the complexation. In addition, pyridine did not perform an absorption band or fluorescence emission in the same region as those of porphyrins.

3.5.1 ^1H NMR Titration

The initial experiment to evaluate the ability of porphyrins as binding receptor and to elucidate the structural change by the complexation began with ^1H NMR titrations.

Binding abilities of three synthesized porphyrins including DMP as free base porphyrin, Zn-DMP as porphyrin metal complex, and Zn-$(TMSE)_2DMP$ as alkyne-linked porphyrin metal complex were examined in their binding abilities by ^1H NMR titration. The ^1H NMR spectra of DMP, Zn-DMP, and Zn-$(TMSE)_2DMP$ with

gradually increasing amounts of pyridine are presented in **Figure 3.26**, **Figure 3.28**, and **Figure 3.30**, respectively. From the ^{1}H NMR titration spectra, chemical shifts of each proton in pyridine and some protons in porphyrins were changed during the titration. These changes are summarized in **Table 3.13-3.15** and the ^{1}H NMR titration curve of DMP, Zn-DMP, and Zn-(TMSE)$_2$DMP with pyridine are illustrated in **Figure 3.27**, **Figure 3.29**, and **Figure 3.31**, respectively.

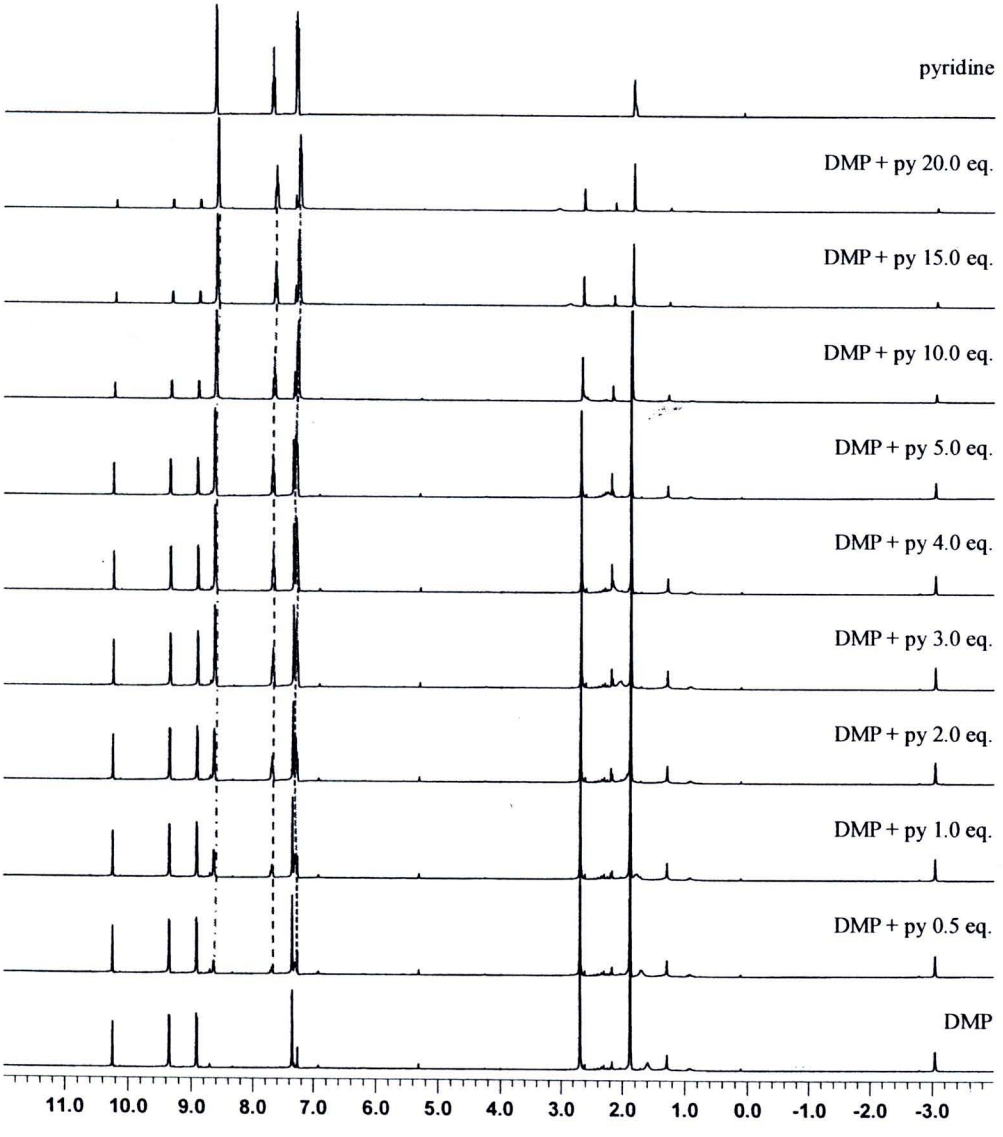

Figure 3.26 The ^{1}H NMR titration spectra of DMP with pyridine in $CDCl_3$

Table 3.13 Changes in chemical shifts of pyridine and DMP protons in the ^{1}H NMR titration of DMP with pyridine in $CDCl_3$

mole ratio of pyridine:porphyrin	δ of pyridine (ppm)			δ of DMP (ppm)		
	ortho-H	*meta*-H	*para*-H	*meso*-H	*β*-H	*β*-H
DMP	-	-	-	10.241	9.347	8.907
0.5 : 1	8.632	7.298	7.686	10.239	9.346	8.906
1 : 1	8.632	7.297	7.684	10.238	9.344	8.905
2 : 1	8.630	7.293	7.680	10.235	9.341	8.902
3 : 1	8.627	7.289	7.676	10.232	9.338	8.899
4 : 1	8.624	7.285	7.673	10.229	9.335	8.896
5 : 1	8.620	7.281	7.668	10.225	9.332	8.893
10 : 1	8.603	7.261	7.649	10.209	9.316	8.879
15 : 1	8.586	7.242	7.629	10.194	9.301	8.865
20 : 1	8.569	7.223	7.610	10.178	9.285	8.850
pyridine	8.611	7.283	7.675	-	-	-

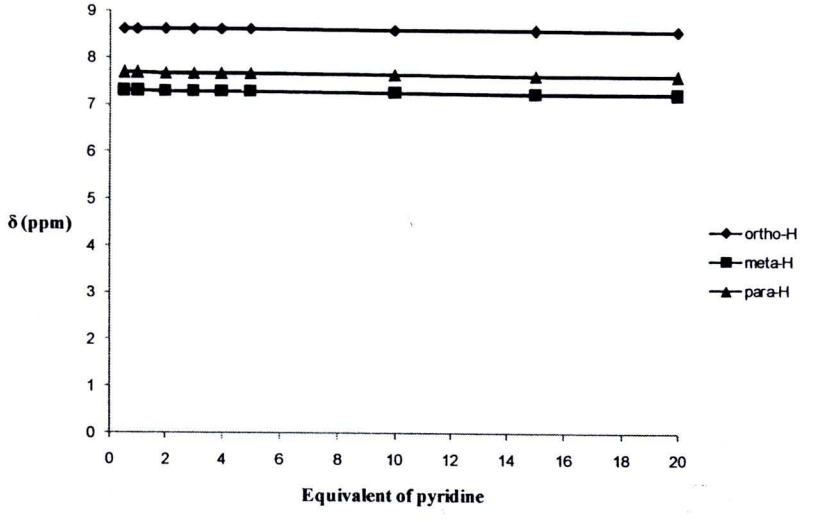

Figure 3.27 The ^{1}H NMR titration curve of DMP with pyridine in $CDCl_3$

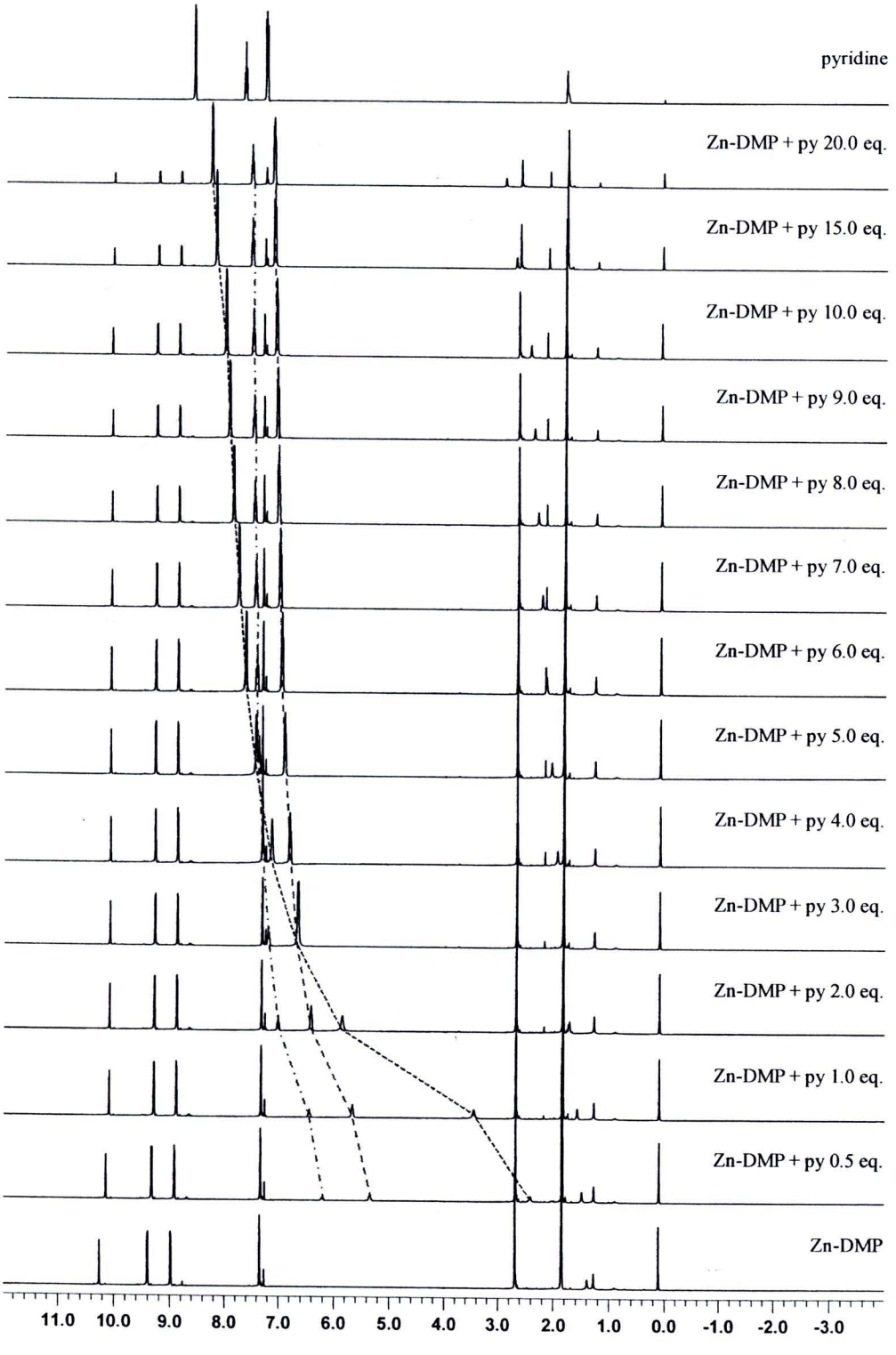

Figure 3.28 The ^{1}H NMR titration spectra of Zn-DMP with pyridine in $CDCl_3$

Table 3.14 Changes in chemical shifts of pyridine and Zn-DMP protons in the ^{1}H NMR titration of Zn-DMP with pyridine in $CDCl_3$

mole ratio of pyridine:porphyrin	δ of pyridine (ppm)			δ of Zn-DMP (ppm)		
	ortho-H	*meta*-H	*para*-H	*meso*-H	β-H	β-H
Zn-DMP	-	-	-	10.257	9.400	8.984
0.5 : 1	2.417	5.351	6.213	10.151	9.336	8.925
1 : 1	3.461	5.671	6.450	10.096	9.302	8.894
2 : 1	5.862	6.421	7.017	10.091	9.298	8.890
3 : 1	6.664	6.676	7.207	10.089	9.296	8.888
4 : 1	7.150	6.820	7.299	10.087	9.293	8.886
5 : 1	7.440	6.909	7.384	10.084	9.290	8.884
6 : 1	7.637	6.968	7.428	10.082	9.288	8.881
7 : 1	7.772	7.007	7.457	10.079	9.285	8.879
8 : 1	7.875	7.037	7.479	10.077	9.283	8.877
9 : 1	7.954	7.059	7.495	10.074	9.280	8.875
10 : 1	8.016	7.076	7.507	10.072	9.277	8.872
15 : 1	8.202	7.120	7.537	10.059	9.264	8.860
20 : 1	8.285	7.133	7.541	10.045	9.250	8.848
pyridine	8.611	7.283	7.675	-	-	-

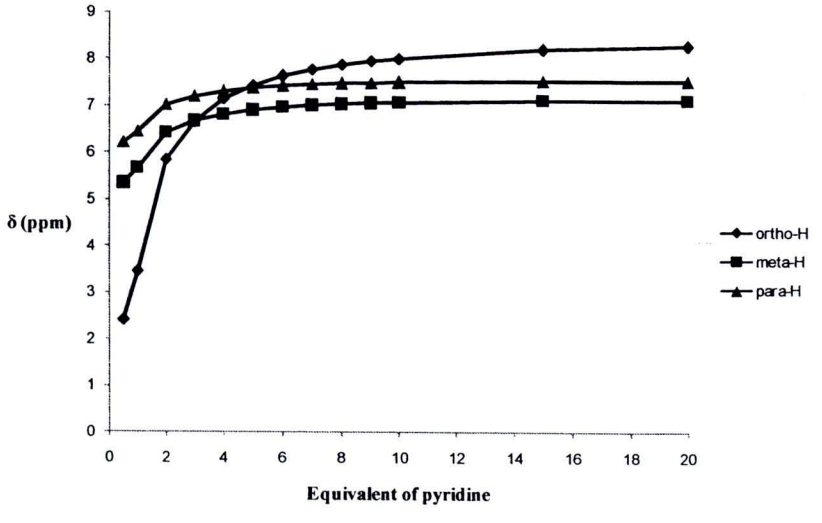

Figure 3.29 The ^{1}H NMR titration curve of Zn-DMP with pyridine in $CDCl_3$

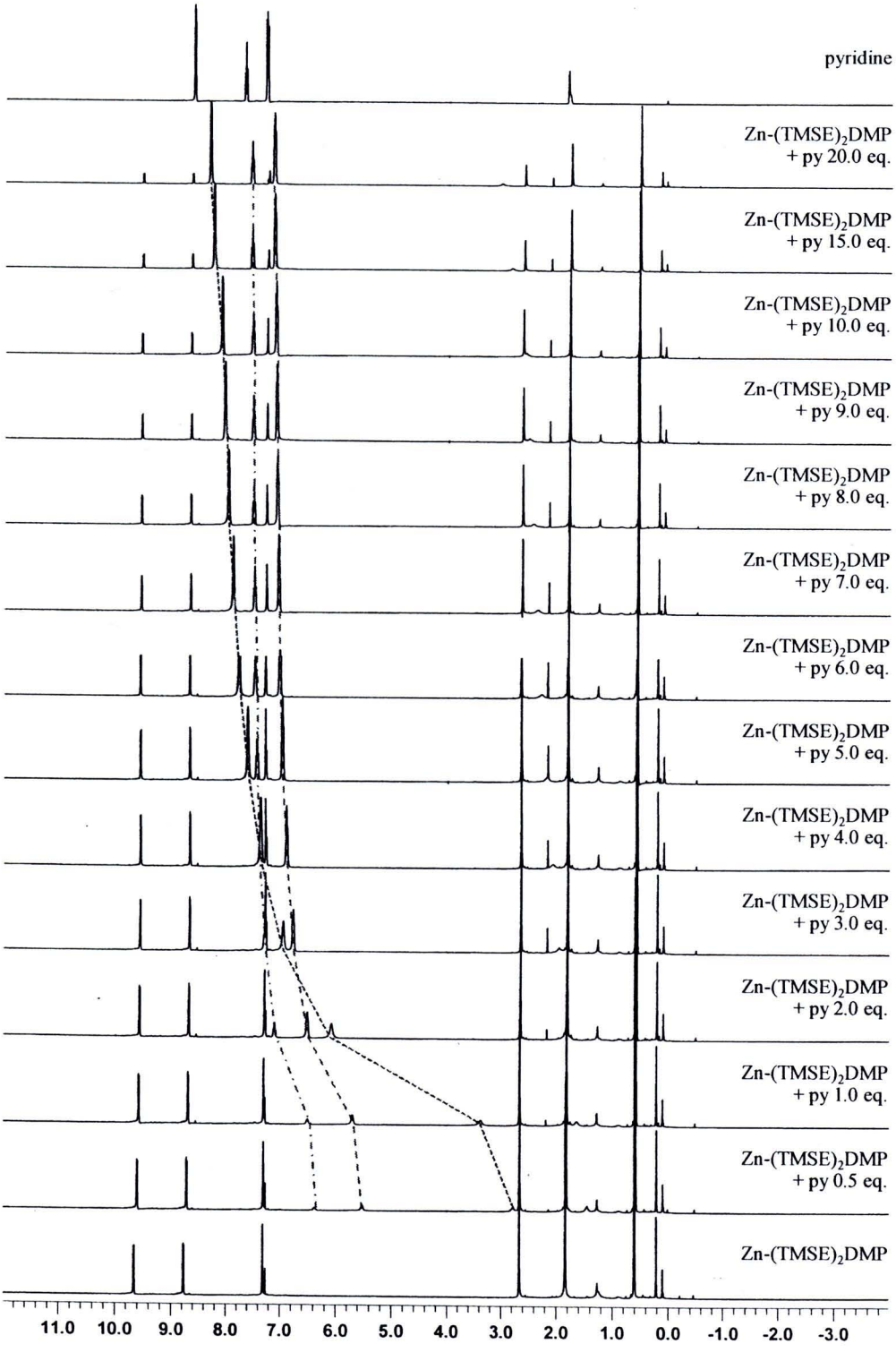

Figure 3.30 The ^{1}H NMR titration spectra of Zn-(TMSE)$_2$DMP with pyridine in $CDCl_3$

Table 3.15 Changes in chemical shifts of pyridine and Zn-(TMSE)$_2$DMP protons in the ^{1}H NMR titration of Zn-(TMSE)$_2$DMP with pyridine in $CDCl_3$

mole ratio of pyridine:porphyrin	δ of pyridine (ppm)			δ of Zn-(TMSE)$_2$DMP (ppm)		
	ortho-H	*meta*-H	*para*-H	*meso*-H	*β*-H	*β*-H
Zn-(TMSE)$_2$DMP	-	-	-	-	9.656	8.767
0.5 : 1	2.775	5.520	6.372	-	9.598	8.710
1 : 1	3.372	5.692	6.494	-	9.567	8.680
2 : 1	6.082	6.512	7.099	-	9.564	8.677
3 : 1	6.954	6.773	7.282	-	9.562	8.674
4 : 1	7.364	6.896	7.380	-	9.561	8.672
5 : 1	7.606	6.967	7.433	-	9.559	8.670
6 : 1	7.764	7.012	7.466	-	9.557	8.668
7 : 1	7.891	7.074	7.491	-	9.555	8.666
8 : 1	7.981	7.072	7.508	-	9.552	8.663
9 : 1	8.039	7.085	7.516	-	9.547	8.657
10 : 1	8.103	7.101	7.528	-	9.547	8.657
15 : 1	8.249	7.133	7.546	-	9.538	8.646
20 : 1	8.313	7.138	7.546	-	9.527	8.634
pyridine	8.611	7.283	7.675	-	-	-

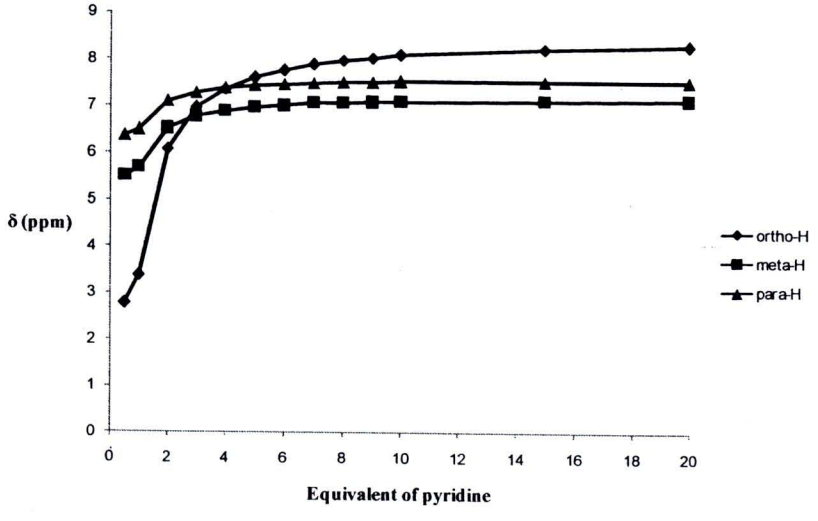

Figure 3.31 The ^{1}H NMR titration curve of Zn-(TMSE)$_2$DMP with pyridine in $CDCl_3$

In the case of DMP, the experiment was carried out as a control reaction. The ^{1}H NMR titration results revealed that there were very slight changes of chemical shifts of protons in both pyridine and DMP. These may be due to weak interactions between DMP and pyridine such as dipole-dipole interaction or π-π interaction.

In contrast, the proton chemical shifts of pyridine in the titration of Zn-DMP and Zn-(TMSE)$_2$DMP clearly showed very upfield shifts compared to those of free pyridine. Moreover, the chemical shifts of some protons, especially at *meso*- and *β*-positions, of Zn-DMP and Zn-(TMSE)$_2$DMP in the presence of increasing amounts of pyridine exhibited gradual upfield shifts. These results indicated that metal ion show an important role as binding site for the ligand coordination and the main interaction between porphyrin metal complexes and pyridine is ion-dipole or coordination interaction.

The most interesting result in the titrations of Zn-DMP and Zn-(TMSE)$_2$DMP with pyridine is the changes of proton chemical shifts of pyridine. When the amounts of pyridine increased, the chemical shifts of protons, especially at *ortho*-positions, of pyridine significantly shifted downfield. These shifts represented the population average between the chemical shifts of free pyridine and those of coordinated pyridine in the system. The coordination of pyridine was relative to the fast exchange reversible dynamic process.

In general, the obtained appeared NMR spectra are basically treated to display a qualitative description of reversible dynamic processes. This topic is often introduced with a discussion of simple two exchange systems: slow and fast exchange. For the slow exchange condition, the NMR spectrum consists of two discrete signals of the bound and free molecules. On the other hand, the NMR spectrum under fast exchange system gives only one signal at the weighted averages chemical shift because the reversible process is faster than the NMR time scale.

From the data of the ^{1}H NMR titration, the structure of porphyrin-pyridine complexes could be also estimated. The coordination of nitrogen atom of pyridine to the Zn(II) ion at the core of porphyrins could be confirmed by the upfield shifts of ^{1}H NMR signals of pyridine relative to those of free pyridine. Particularly, the signals of *ortho*-protons of pyridine exhibited the largest changes because these protons are closest to the core of porphyrin rings which can be affected violently by the ring current effect of porphyrins. However, at this stage there is an inadequate amount of data to predict the binding stoichiometry of porphyrin-pyridine complexes. Therefore,

the continuous variation method (the Job's plots analysis) was evaluated as an alternative to determine the binding stoichiometry of the complexes. The Job's plots were plotted between the mole fraction of pyridine in the mixture and $\Delta\delta(1-x)$ calculated from the chemical shift changes ($\Delta\delta$) for the corresponding protons multiplied by their inverse mole fraction (1-x). In this determination, the chemical shift changes of the ortho-protons of pyridine were chosen to use as the corresponding protons because of their outstanding changes.

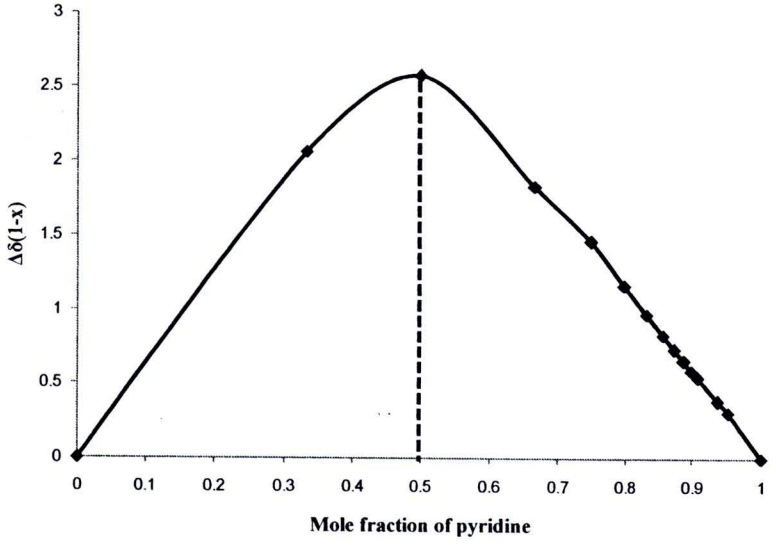

Figure 3.32 The Job's plot of the complexation of Zn-DMP with pyridine

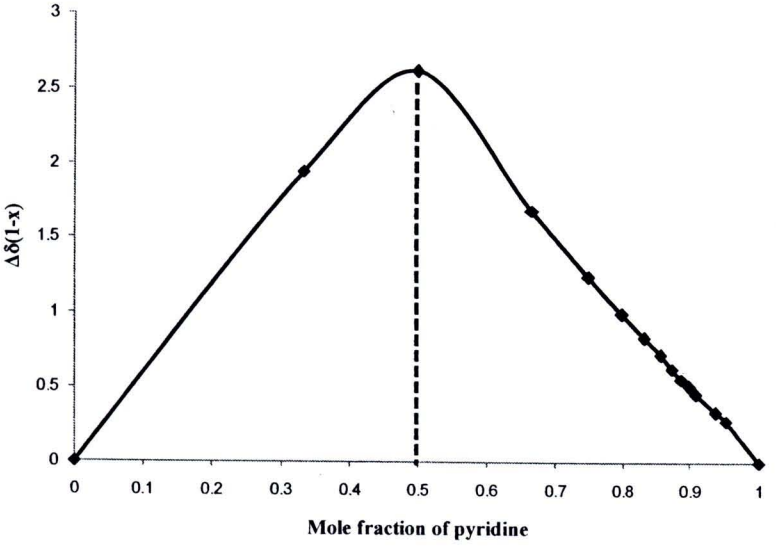

Figure 3.33 The Job's plot of the complexation of Zn-$(TMSE)_2$DMP with pyridine

The Job's plots of the complexation of Zn-DMP (**Figure 3.32**) and Zn-(TMSE)$_2$DMP (**Figure 3.33**) exhibited relatively symmetrical curves with maximum points at 0.5 mole fraction. It concerned the formation of 1:1 porphyrin-pyridine complexes. The proposed structure of 1:1 porphyrin-pyridine complexes is as illustrated in **Figure 3.34**.

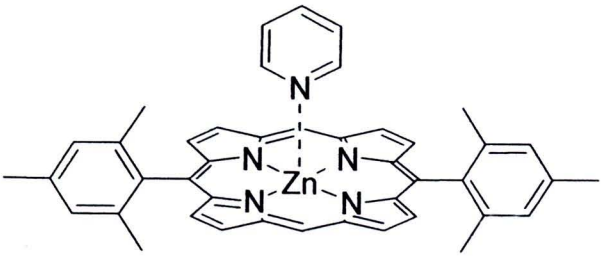

Figure 3.34 The proposed structure of 1:1 porphyrin-pyridine complex

In addition, attempts have been made to confirm the 1:1 complexation of porphyrins with pyridine by MALDI-TOF mass spectrometry. Unfortunately, only the molecular ion peaks of porphyrins were observed, whereas those of porphyrin-pyridine complexes could not be detected. It may be because the complexations of Zn-DMP and Zn-(TMSE)$_2$DMP with pyridine are not strong enough to be detected under high energy conditions of the laser ionization.

3.5.2 UV-Visible Titration

The UV-visible titrations of six porphyrins including Zn-DMP, Zn-Br$_2$DMP, Zn-(TMSE)$_2$DMP, Zn-E$_2$DMP, Zn-(PE)$_2$DMP, and Mn-DMP with pyridine were carried out (**Figure 3.35-3.40**) in order to evaluate the potential of these porphyrins as optical sensors.

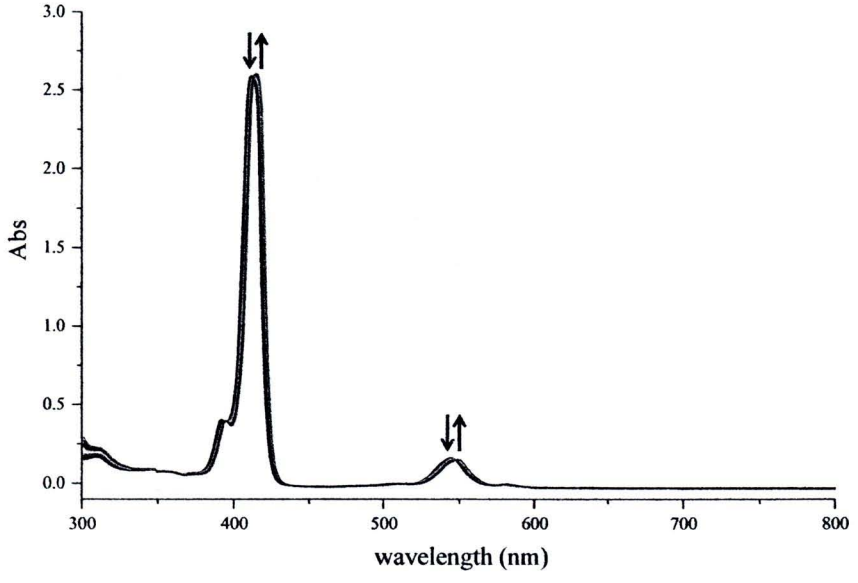

Figure 3.35 The UV-visible titration spectra of Zn-DMP (10^{-5} M in THF) with pyridine at 25 °C

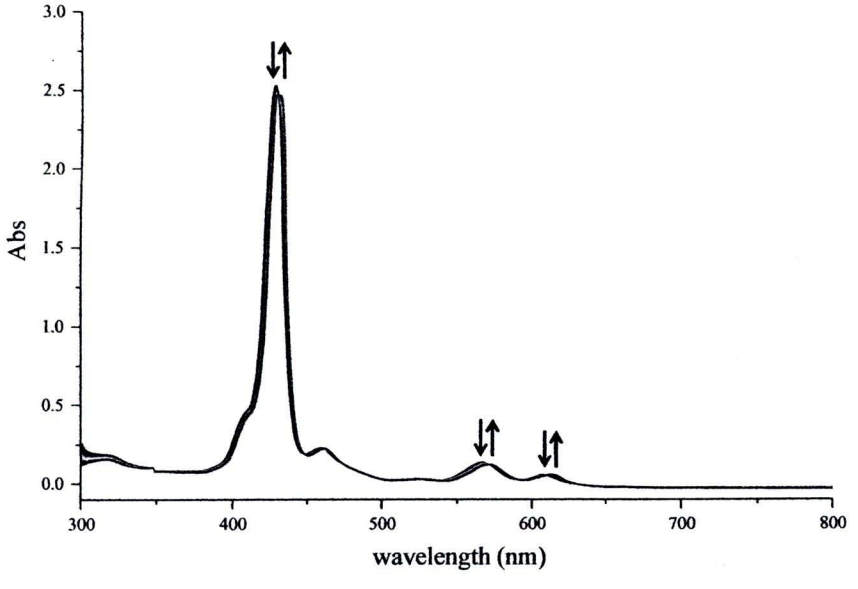

Figure 3.36 The UV-visible titration spectra of Zn-Br_2DMP (10^{-5} M in THF) with pyridine at 25 °C

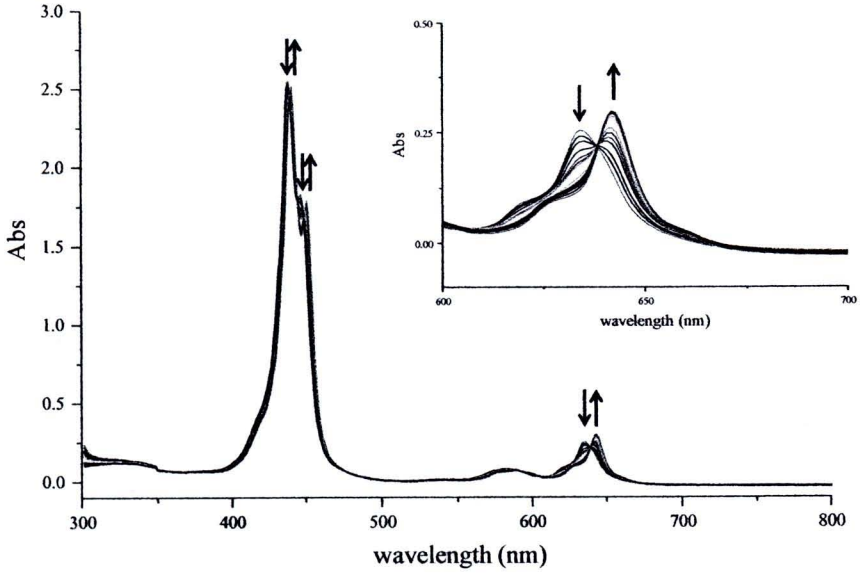

Figure 3.37 The UV-visible titration spectra of Zn-$(TMSE)_2$DMP (10^{-5} M in THF) with pyridine at 25 °C

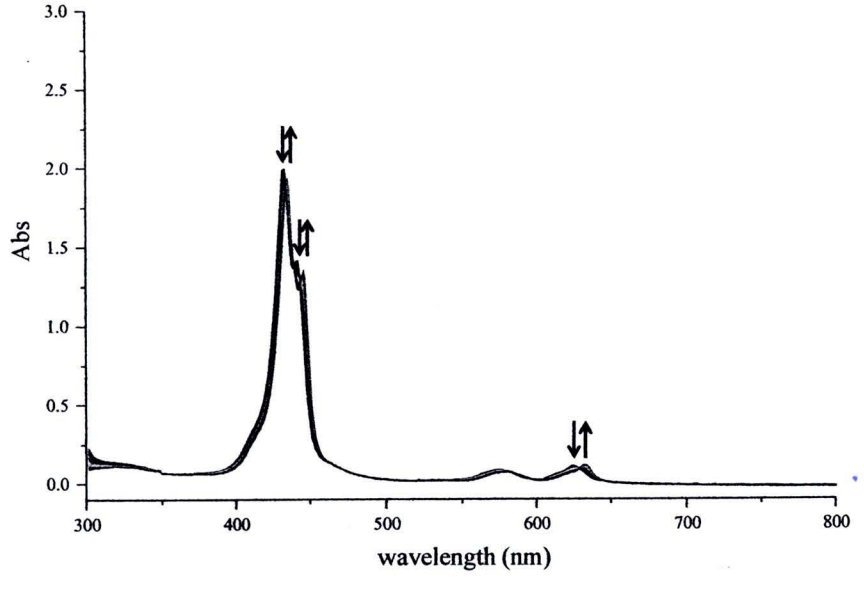

Figure 3.38 The UV-visible titration spectra of Zn-E_2DMP (10^{-5} M in THF) with pyridine at 25 °C

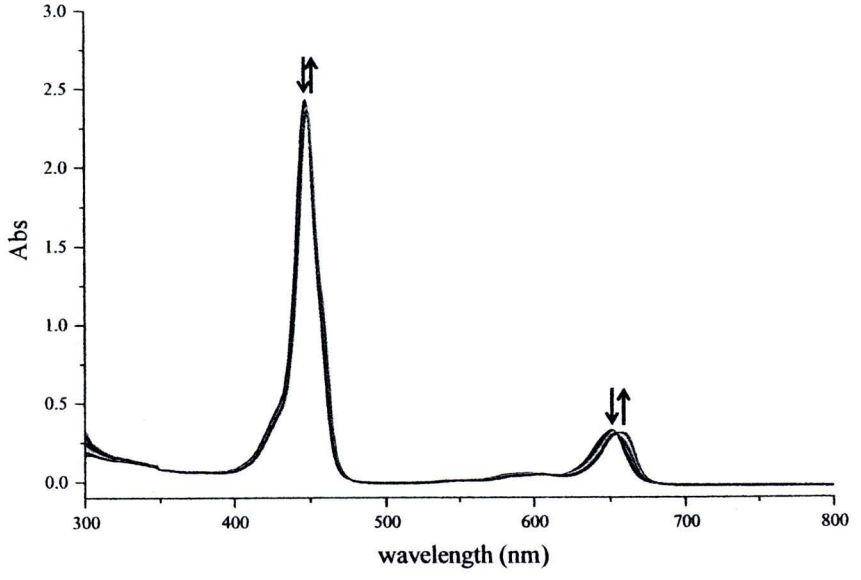

Figure 3.39 The UV-visible titration spectra of Zn-$(PE)_2$DMP (10^{-5} M in THF) with pyridine at 25 °C

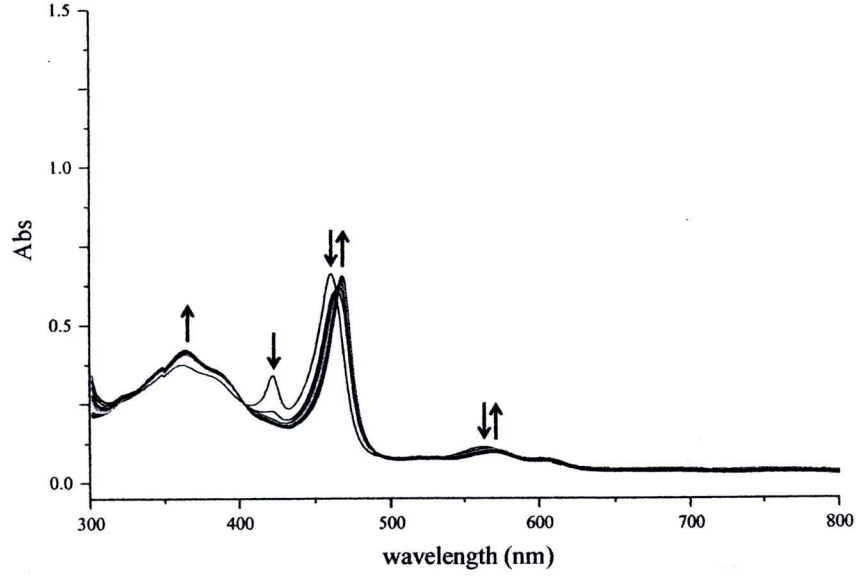

Figure 3.40 The UV-visible titration spectra of Mn-DMP (10^{-5} M in THF) with pyridine at 25 °C

All of the UV-visible titration experiments exhibited relatively similar results. Upon the addition of pyridine, both Soret band and Q bands in the absorption spectra were induced to the red shifted absorption bands. The new red shifted bands are characteristics of porphyrin-pyridine complexes. These observations are ascribed to the destabilization of the HOMO with a little effect on the LUMO of porphyrins arising from a flow of charge from the axial ligand to the porphyrin ring through the metal ion [76]. Furthermore, clear isosbestic points which are indicatives of sequential two-state equilibria were also observed in every experiment.

As shown in the UV-visible titration spectra, the absorption bands of alkyne-linked porphyrins such as Zn-$(TMSE)_2$DMP, Zn-E_2DMP, and Zn-$(PE)_2$DMP displayed remarkably greater changes, especially at Q bands, corresponding to those of Zn-DMP and Zn-Br_2DMP. This examination suggested that alkyne-linked porphyrin metal complexes exhibit higher potential for binding materials in optical sensors than their porphyrin building blocks.

Interestingly, the UV-visible titration spectra of Mn-DMP presented the most outstanding results relative to those of porphyrin zinc complexes. It concerned the large decrease of absorbance at 422 nm and remarkable red shifts from 460 to 468 nm since the first addition of pyridine. These results suggested that porphyrin manganese complexes show higher sensitivity for the binding of ligand than porphyrin zinc complexes.

3.5.3 Fluorescence Titration

The fluorescence titration spectra of three synthesized porphyrins including Zn-DMP, Zn-$(TMSE)_2$DMP, and Zn-$(PE)_2$DMP with pyridine are presented in **Figure 3.41-3.43**, respectively.

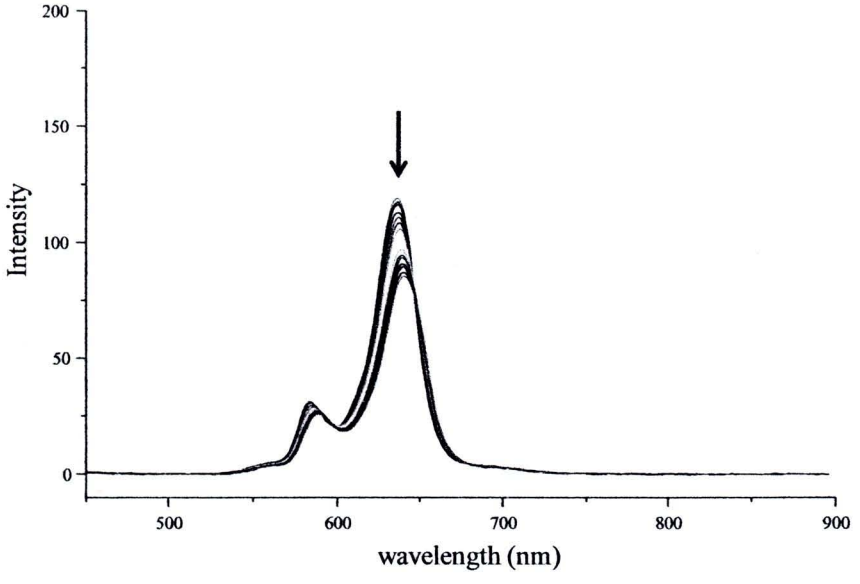

Figure 3.41 The fluorescence titration spectra of Zn-DMP (10^{-5} M in THF) with pyridine at ambient temperature

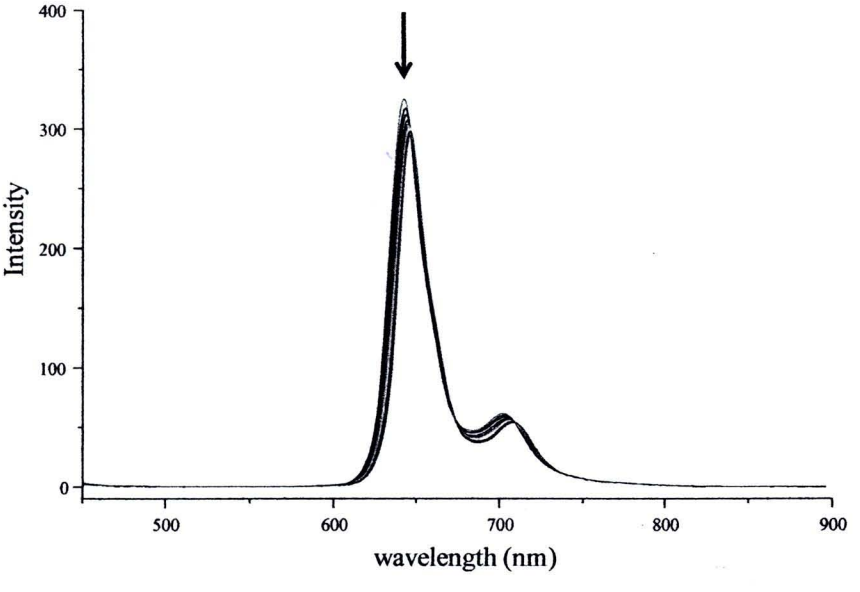

Figure 3.42 The fluorescence titration spectra of Zn-$(TMSE)_2$DMP (10^{-5} M in THF) with pyridine at ambient temperature

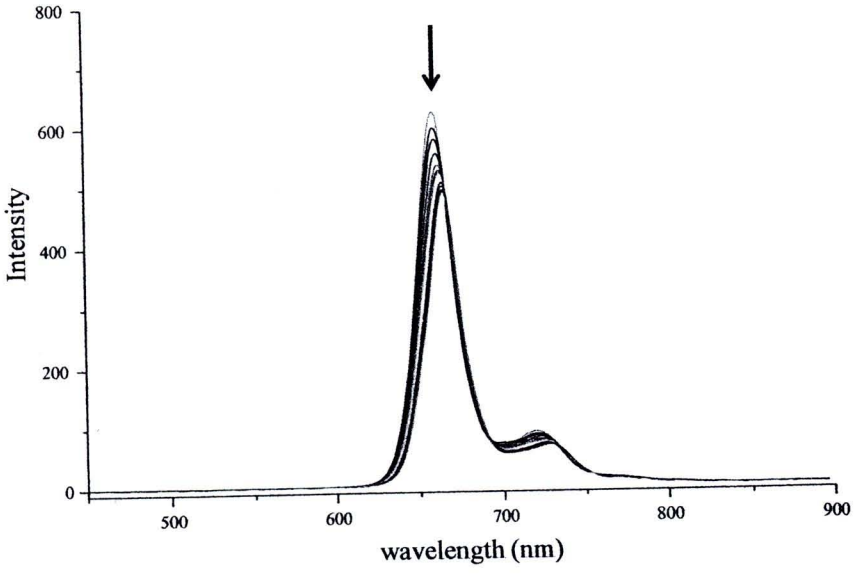

Figure 3.43 The fluorescence titration spectra of Zn-$(PE)_2$DMP (10^{-5} M in THF) with pyridine at ambient temperature

All fluorescence titration spectra of porphyrins showed changes in emission intensity with a gradual increase in the amount of pyridine. Upon the addition of pyridine, the intensity of fluorescence emission continually decreased with a concomitant of slight red shifts. Similar to the UV-visible titration experiments, these changes can arise from the destabilization of the HOMO of porphyrins. However, there are no significant differences in the changes of titration spectra of all observed porphyrins with pyridine.